MINISTERE DE L'ENSEIGNEMENT SUPERIEUR ET DE LA RECHERCHE SCIENTIFIQUE

Felix Houphouet-Boigny university

N°: 659

UNITE DE FORMATION ET DE RECHERCHE SCIENCES DES STRUCTURES DE LA MATIERE ET DE TECHNOLOGIE

RÉPUBLIQUE DE CÔTE D'IVOIRE
UNION - DISCIPLINE - TRAVAIL

Institute of Energy and Climate Research – Theory and Computation of Energy Materials (IEK-13), Forschungszentrum Jülich

SPONSORED BY THE

# MASTER IN RENEWABLE ENERGY AND CLIMATE CHANGE

**SPECIALITY:** PRODUCTION AND TECHNOLOGIES OF GREEN HYDROGEN

## MASTER THESIS:

## Topic:

**MODEL-BASED COMPARATIVE ASSESSMENT OF FREQUENCY RESPONSE DIAGNOSTIC METHODS FOR ELECTROCHEMICAL ENERGY DEVICES**


Presented on September 2023 by:

**Mamadou Moustapha KEBE**


**JURY:**

| | | |
|---|---|---|
| Prof. OBROU Olivier | **President** | Professor at UFHB |
| Prof. ESSI Marc Marie-Maurice Mélèdge | **Examiner** | Professor at UFHB |
| Dr. KOUA Kamenan Blaise | **Supervisor** | Lecturer at UFHB |
| Prof. Dr. rer. nat. Michael H. EIKERLING | **Co-Supervisor** | Chair of IEK-13 at FZJ / Professor at RWTH Aachen University |

**Erreur ! Utilisez l'onglet Accueil pour appliquer Heading 1 au texte que vous souhaitez faire apparaître ici.**

I dedicate this work to the cherished individuals who have played pivotal roles in my life's journey. To my beloved mother, Maryatou NDIOR, who has been both my guiding light and my rock throughout, and to my late father, Modou KEBE, whose memory continues to inspire me. To my brothers, for their steadfast support, and to my devoted uncle, Babacar FAME, who has been a constant pillar of encouragement throughout my academic path. To my future wife, Katia Aminata KONE, whose consistent support has sustained me during this journey, and to my treasured friends, who have shared in both my challenges and triumphs. This work stands as a testament to the love, encouragement, and belief in me that each of you has provided.

**Erreur ! Utilisez l'onglet Accueil pour appliquer Heading 1 au texte que vous souhaitez faire apparaître ici.**

# ACKNOWLEDGEMENTS

I would like to express my sincere gratitude and appreciation to all those who have contributed to the successful completion of my master's thesis.

First, I am immensely thankful to the funder, the German Federal Ministry of Education and Research (BMBF), and the West African Science Service Centre on Climate Change and Adapted Land Use (WASCAL) and all their partners for providing me with the incredible opportunity of this scholarship.

I am also deeply grateful to the WASCAL teams in Niger, led by Prof. Adamou RABANI, and in Cote d'Ivoire, led by Dr. Konan Edouard KOUASSI, for their unwavering support throughout the first and second years of this master program. Their endless encouragement and assistance, being fathers and brothers and not just directors of programs, have been invaluable in making this academic journey a success.

I would like to express my sincere gratitude for the endless support and guidance provided by my supervisors, Dr. Blaise Kamenan KOUA and Prof. Dr. rer. nat. Michael EIKERLING, throughout this research journey. My special thanks go to Prof. Dr. rer. nat. Michael EIKERLING whose expertise, guidance, and encouragement have been instrumental in shaping the direction and quality of this thesis.

I offer my sincere thanks to Dr. Thomas KADYK for his patience, commitment, and expert guidance through all this thesis, his mentorship has been invaluable. Thanks also to Ying SUN for everything she has done, her guidance, availability, and prompt feedback have been indispensable in shaping the success of this thesis, to Dr. Andrei KULIKOVSKY as well for all the help and contributions in my research. Words cannot describe how grateful I am for your support and guidance. Thanks also to the entire team of IEK-13 at Forschungszentrum Jülich for creating a warm and supportive research environment, their kindness and welcoming attitude have made this experience all the more rewarding.

I also extend my gratitude to the esteemed members of the jury, starting from Prof. OBROU Olivier the president, Prof. ESSI Marc Marie-Maurice Mélèdge the examiner, Dr. KOUA Kamenan Blaise my supervisor, and Prof. Dr. rer. nat. Michael EIKERLING my co-supervisor, for their time and valuable insights during the evaluation of this thesis.

Lastly, I want to thank my family and loved ones for their support, encouragement, and understanding. Their confidence in my abilities has been a constant source of motivation.

This thesis would not have been possible without the dedication and encouragement of all those mentioned above. Your guidance and kindness have made a profound impact, and I

am excited to carry the lessons learned into my future endeavors. Thank you all from the bottom of my heart.

**Erreur ! Utilisez l'onglet Accueil pour appliquer Heading 1 au texte que vous souhaitez faire apparaître ici.**

# ABSTRACT

Electrochemical energy devices, including electrolyzers, batteries, and fuel cells, hold significant promise as sustainable solutions for energy storage and conversion. Among fuel cells, polymer electrolyte fuel cells are currently the most widely studied technology and the most promising candidate for sustainable power generation in a wide range of applications. To ensure their reliable operation and optimal performance, accurate diagnostic methods are essential. Frequency response analysis has proven to be a valuable tool for evaluating the dynamic behavior and internal characteristics of electrochemical energy devices.

The thesis starts with a comprehensive literature review that focuses on diagnostic methods for frequency response analysis in electrochemical energy devices, especially in polymer electrolyte fuel cells. Various approaches, including electrochemical impedance spectroscopy, electrochemical pressure impedance spectroscopy, concentration-alternating frequency response analysis, and concentration admittance spectroscopy, are explored.

The aim of this master thesis is to develop and test a method to characterize and quantitatively compare different frequency response diagnostic methods for polymer electrolyte fuel cells.

In order to find the best frequency response analysis method or combination of methods, a framework based on linear system theory is used to evaluate the strength or weakness of a given method. An existing analytical solution of a simple electrochemical impedance spectroscopy model of the cathode catalyst layer of a polymer electrolyte fuel cell is utilized to characterize observability, controllability, and parameter sensitivity. A transmission line model of the cathode catalyst layer is used as well to calculate the impedance response and compared with this analytical solution.

Next, a transmission line model that takes into account oxygen transport in the cathode catalyst layer is constructed to calculate the impedance response and compared it with an existing analytical result.

**Key words:** Polymer electrolyte fuel cells - frequency response analysis - electrochemical impedance spectroscopy - diagnostic methods - physical model - transmission line model.

# RESUME

Les dispositifs énergétiques électrochimiques, notamment les électrolyseurs, les batteries et les piles à combustible, sont très prometteurs en tant que solutions durables pour le stockage et la conversion de l'énergie. Parmi les piles à combustible, celles à membrane électrolyte polymère sont actuellement les technologies les plus étudiées. Elles sont considérées comme les candidats les plus prometteurs pour la production d'énergie durable dans un large éventail d'applications. Toutefois, pour garantir leur fonctionnement fiable et leur optimale performance, il est essentiel de disposer de méthodes de diagnostic précises. L'analyse de la réponse en fréquence s'est avérée être un outil précieux pour évaluer le comportement dynamique et les caractéristiques internes des dispositifs d'énergie électrochimique.

Ce mémoire présente une analyse documentaire complète, axée sur les méthodes de diagnostic pour l'analyse de la réponse en fréquence dans les dispositifs d'énergie électrochimique, en particulier dans les piles à combustible à membrane électrolyte polymère. Diverses approches, notamment la spectroscopie d'impédance électrochimique, la spectroscopie d'impédance de pression électrochimique, l'analyse de la réponse en fréquence en fonction de la concentration et la spectroscopie d'admittance de concentration ont été explorées.

Le but de ce mémoire est d'améliorer la compréhension et l'application des méthodes de diagnostic de la réponse en fréquence pour les dispositifs d'énergie électrochimique, avec un accent particulier sur les piles à combustible à membrane électrolyte polymère.

Afin de trouver la meilleure méthode d'analyse de la réponse en fréquence ou la meilleure combinaison de méthodes, un cadre basé sur la théorie des systèmes linéaires est utilisé pour évaluer la force ou la faiblesse d'une méthode donnée. Une solution analytique existante d'un simple modèle de spectroscopie d'impédance électrochimique de la couche catalytique de la cathode d'une pile à combustible à membrane électrolyte polymère est utilisée pour caractériser l'observabilité, la contrôlabilité et la sensibilité des paramètres. Un modèle de ligne de transmission de la couche catalytique cathodique est également développé et comparé à ce modèle analytique.

Ensuite, un modèle de ligne de transmission, prenant en compte le transport de l'oxygène dans la couche catalytique de la cathode, est construit pour calculer la réponse d'impédance et comparé à un modèle physique existant.

**Erreur ! Utilisez l'onglet Accueil pour appliquer Heading 1 au texte que vous souhaitez faire apparaître ici.**

**Mots clés :** Piles à combustible à membrane électrolytique polymère - analyse de la réponse en fréquence - spectroscopie d'impédance électrochimique - méthodes de diagnostic - modèle physique - modèle de ligne de transmission.

**Erreur ! Utilisez l'onglet Accueil pour appliquer Heading 1 au texte que vous souhaitez faire apparaître ici.**

# TABLE OF CONTENT

**Erreur ! Utilisez l'onglet Accueil pour appliquer Heading 1 au texte que vous souhaitez faire apparaître ici.**

**Erreur ! Utilisez l'onglet Accueil pour appliquer Heading 1 au texte que vous souhaitez faire apparaître ici.**

# LIST OF FIGURES

**Erreur ! Utilisez l'onglet Accueil pour appliquer Heading 1 au texte que vous souhaitez faire apparaître ici.**

# LIST OF TABLES

**Erreur ! Utilisez l'onglet Accueil pour appliquer Heading 1 au texte que vous souhaitez faire apparaître ici.**

# ACCRONYMS AND ABBREVIATION

CAS ..... Concentration Admittance Spectroscopy
CCPs ..... Current Collector Plates
cFRA ..... Concentration-alternating Frequency Response Analysis
CL ..... Catalyst Layers
EC ..... Equivalent Circuit
ECM ..... Equivalent Circuit Model
EDL ..... Electrochemical Double Layer
EIS ..... Electrochemical Impedance Spectroscopy
EPIS ..... Electrochemical Pressure Impedance Spectroscopy
ETIS ..... Electro-Thermal Impedance Spectroscopy
FCs ..... Fuel Cells
FRA ..... Frequency Response Analysis
GDL ..... Gas Diffusion Layer
GHGs ..... Greenhouse Gases
HECII ..... Hydro-Electrochemical Impedance Imaging
HOR ..... Hydrogen Oxidation Reaction
LIT ..... Lock-in Thermograpy
MEA ..... Membrane Electrode Assembly
MPL ..... Microporous Layer
NAFION ..... Sodium (Na) and Fluorine (F) Ions
ORR ..... Oxygen Reduction Teaction
PEM ..... Polymer Electrolyte Membrane
PEFC ..... Polymer Electrolyte Fuel Cell
PTFE ..... Polytetrafluoroethylene
PTL ..... Porous Transport Layer
sFRA ..... Species Frequency Response Analysis
SISO ..... Single Input Single Output
TLM ..... Transmission Line Model

**Erreur ! Utilisez l'onglet Accueil pour appliquer Heading 1 au texte que vous souhaitez faire apparaître ici.**

# LIST OF SYMBOLS

| | |
|---|---|
| $\tilde{}$ | marks dimensionless variables |
| $A$ | state space matrix |
| $B$ | observability matrix |
| $b$ | Tafel slope $b$ , V |
| $C$ | controllability matrix |
| $c$ | oxygen concentration, mol $cm^{-3}$ |
| $C_{dl}$ | CL double layer capacitance, F $cm^{-3}$ |
| $c_{ref}$ | reference oxygen concentration, mol $cm^{-3}$ |
| $D$ | transmission matrix |
| $D_{ox}$ | CCL oxygen diffusivity, $cm^2\ s^{-1}$ |
| $F$ | Faraday constant, C $mol^{-1}$ |
| $G$ | generic function |
| $H$ | generic transfer function |
| $i_*$ | exchange current density, A $cm^{-3}$ |
| $K$ | generic function |
| $j$ | current density, A $cm^{-2}$ |
| $l_t$ | CL thickness, cm |
| $R$ | gas constant, J $mol^{-1}$ $K^{-1}$ |
| $r$ | residual |
| $R_{ct}$ | charge transfer resistance, Ω $cm^2$ |
| $R_m$ | membrane resistance, Ω $cm^2$ |
| $S_R$ | relative sensitivity |
| $T$ | temperature, K |
| $t$ | time, s |
| $U$ | input vector |
| $X$ | state variable vector |
| $x$ | distance from the membrane, cm |
| $Y$ | output vector |
| $Z$ | impedance, Ω $cm^2$ |

***Greek Symbols***

| | |
|---|---|
| $\alpha$ | transfer coefficient |
| $\beta$ | normal input vector |
| $\gamma$ | normal output vector |
| $\lambda$ | eigenvalue |
| $\Lambda$ | matrix of the eigenvalues |
| $\eta$ | half-cell overpotential, V |
| $\sigma_p$ | proton conductivity, $\Omega^{-1}$ $cm^{-1}$ |
| $\omega$ | angular frequency, rad $s^{-1}$ |

***Superscripts***

| | |
|---|---|
| 0 | steady–state value |
| 1 | small–amplitude perturbation |

***Subscripts***

| | |
|---|---|
| 0 | membrane/CCL interface |
| 1 | CCL/GDL interface |
| $ccl$ | cathode catalyst layer |
| $d$ | diagonal |
| $ox$ | oxygen |
| $p$ | proton |
| $w$ | Warburg |

# INTRODUCTION

# INTRODUCTION

The 20th century is marked by the revolutionary technological growth around the world. Nevertheless, this modern world has engendered a considerable increase in the energy demand [1, 2]. Fossil fuels constitute the primary energy resource utilized to meet this demand. Unfortunately, many challenges result from the exploitation of this energy source. They are exhaustible overtime and their use affects the air quality as well as increases the concentration of greenhouse gases (GHGs) in the atmosphere, the principal cause of climate change [3].

All these factors inspired scientists around the world to align efforts and policy makers to sign the Paris agreement in 2015, committing to reduce the GHG emissions [4] by searching for better alternatives, hence the energy transition. It consists of replacing fossil fuels with energy sources that are sustainable and climate-friendly [5]. However, these green energy sources have their challenges. For instance, the availability of resources for most of the renewable energies is fluctuating. Indeed, they depend on external factors, for example, days without wind or sun can affect the production of energy from those sources. The development of a sustainable energy system is then required for supporting the renewable energy deficit when necessary, and storing the excess of it when possible [6].

The field of sustainable energy technologies has witnessed the emergence of electrochemical energy devices, such as batteries, electrolyzers and fuel cells, as promising devices for energy storage and conversion [7]. Among these fuel cells, especially Polymer Electrolyte Fuel Cells (PEFC), have gained importance in various applications, including mobile and portable applications, due to their high energy conversion efficiency and environmental friendliness [8]. To ensure their reliable development, fabrication, operation and optimal performance, accurate diagnostic methods are essential [9].

Frequency response analysis (FRA) has proven to be a valuable tool for evaluating the dynamic behavior and internal characteristics of electrochemical energy devices. It consists of harmonically perturbing the studied system: an input signal of a single frequency is applied and the output signal (or multiple signals) is analyzed [9]. FRA allows for the extraction of crucial information related to impedance, capacitance, and other electrochemical parameters. This information enables to gain deep insights into the device's health, identification of degradation mechanisms, and optimization of their operation.

For FRA, current and voltage are often used as perturbation signals due to their easy experimental accessibility and high accuracy in application and measurement. However, other input or output signals like pressure, concentration of reactant, flow rate, humidity or

temperature can be also used. This creates opportunities to explore novel diagnostic techniques [9].

In order to find the most insightful FRA method or combination of methods, or to explore the potential of new methods, the model-based analyses of controllability, observability and sensitivity are pertinent tools. A framework based on linear system theory was developed, which is suitable to compare different input and output signal combinations [10]. In this way, the strengths and weaknesses of different methods can be evaluated before investing in experimental instrumentation. In order to evaluate the strength of a given method, relative sensitivities were introduced as a measure and used for the evaluation of Electrochemical Pressure Impedance Spectroscopy (EPIS) [11], while other foci were Species Frequency Response Analysis (sFRA) [12] and Concentration Admittance Spectroscopy (CAS) [13]. By analyzing the relative sensitivity as a function of the input frequency, the optimal frequency band to extract a certain parameter can be determined. This helps optimizing the optimal frequency range and it can be used to combine different methods. Further, design of experiment methods can be used to optimize the distribution of the input frequency to achieve desired diagnostic tools, e.g., maximize accuracy for a given measurement time, or to minimize measure time, while maintaining a desired accuracy [14].

For this purpose, the following tasks have been performed in this Master's thesis:

- A simple Electrochemical Impedance Spectroscopy (EIS) model, for which an analytical solution exists [15], has been employed to characterize the observability, controllability and the parameter sensitivity (e.g. as function of frequency as done in [13]) using the background in linear systems theory as outlined by Sorrentino et al. [10], in Section 3.1.
- After these tools for characterizing EIS analysis methods had been established, we have expanded the analysis by constructing a transmission line model (TLM) for the cathode catalyst layer (CCL) and compute the impedance response taking into account oxygen transport limitations. A sensitivity analysis has been performed as well.

The remainder of this thesis is structured as follows: Chapter 1 provides a detailed literature review of fuel cells and their frequency response diagnostic methods. Chapter 2 describes the methodology employed. Chapter 3 presents the results obtained, followed by a discussion. Finally, the thesis concludes with a summary of results, perspectives for future research, and implications for the field of electrochemical energy devices.

# CHAPTER 1:

# LITERATURE REVIEW

# CHAPTER 1: LITERATURE REVIEW

In this chapter, we offer a comprehensive review on Polymer Electrolyte Fuel Cells (PEFC), which is the central focus of our research. This section forms the basis of our thesis work. We begin by briefly discussing different types of fuel cells and noting their distinctions. Subsequently, we conduct a detailed examination of PEFC, covering its structure, working principle, and dynamic behavior. Additionally, we provide a brief introduction to Frequency Response Analysis (FRA) as a dynastic method for studying PEFC, and conclude this section by discussing various diagnostic techniques for PEFC.

## 1.1 FUEL CELLS

The discovery of Fuel Cells (FCs) can be attributed to sir William Robert Grove and Christian Friedrich Schönbein, who first identified them in 1838 [16]. FCs are devices that convert chemical energy, stored in a fuel (in this research hydrogen is used as a fuel) and an oxidant (oxygen, e.g., from air), directly into electrical energy, while simultaneously producing water as a product and generating heat [17]. The hydrogen is supplied from a storage tank, while the oxygen is supplied by ambient air. However, in certain applications pure oxygen supply is required. Figure 1 displays a schematic illustrating the inputs and outputs of a fuel cell.

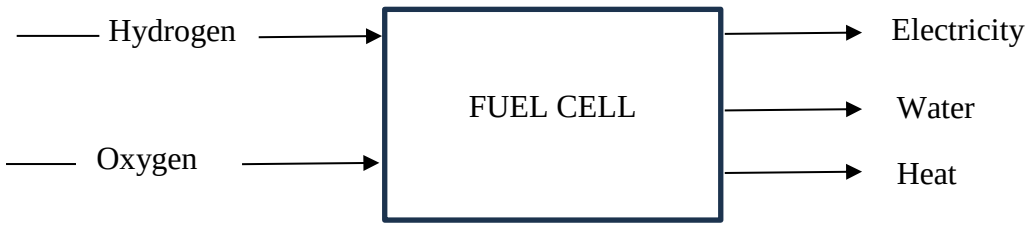


**Figure 1** Fuel cell inputs and outputs.

The electrical energy resulting from the chemical reaction can be used externally by an applied load. Fuel cells play a key role in the mitigation of greenhouse gas emissions across various applications due to their simplicity, high power density, scalability, flexibility, dynamic operation, possibility to use different fuels, high efficiency, and environmentally friendly operability [18].

There are different types of fuel cells. Generally, they are categorized based on their operational temperature or the nature of their electrolyte. Table 1 gives an overview of the different types of fuel cells on which researchers are more focused.

**Table 1:** Different types of fuel cells [18].

| FUEL CELL TYPE | Mobile ion | Operating temperature | Applications and notes |
|---|---|---|---|
| **Alkaline (AFC)** | $OH^-$ | 50 – 200º C | Used in space vehicles, e.g. Apollo, Shuttle. |
| **Proton exchange membrane (PEFC)** | $H^+$ | 30 – 100º C | Vehicles and mobile applications, and for lower power combined heat and power (CHP) systems |
| **Direct methanol (DMFC)** | $H^+$ | 20 – 90º C | Suitable for portable electronic systems of low power, running for long times |
| **Phosphoric acid (PAFC)** | $H^+$ | ~220º C | Large numbers of 200-kW CHP systems in use. |
| **Molten carbonate (MCFC)** | $CO_3^{2-}$ | ~650º C | Suitable for medium- to large-scale CHP systems, up to MW capacity |
| **Solid oxide (SOFC)** | $O^{2-}$ | 500 – 1000º C | Suitable for all sizes of CHP systems, 2 kW to multi-MW. |

Among these fuel cells, the polymer electrolyte fuel cell, also called proton exchange membrane fuel cell (PEFC) is currently the most widely studied technology. This thesis focuses on this type of fuel cell.

## 1.2 POLYMER ELECTROLYTE FUEL CELLS

The concept of the PEFC was first conceived in the 1960s at General Electric in the United States. It played a significant role in NASA's Project Gemini during the initial stages of the United States' space program. However, the research and advancement of PEFC technology did not receive significant attention or funding from the federal government, specifically the US Department of Energy (DOE), and it was replaced by alkaline fuel cells during the Apollo and subsequent space vehicles. This was primarily due to severe obstacles associated with water management, hydrogen storage and transportation, insufficient lifetime (only about 500 h for the first versions used in the NASA Gemini spacecraft [18]), and high costs that were inherent to PEFC [19]. Nonetheless, PEFCs are considered the most promising contenders for sustainable power generation in various areas such as automotive, distributed power systems, and portable electronics, ensuring a greener future [20] due to its simplicity, viability, quick start-up, high energy conversion efficiency, low operating temperature, high current density, zero emissions and flexible useability in various applications. Due to the potential impact of transportation on the environment, scientists and engineers, primarily within the automobile industry have dedicated their efforts to the advancement and optimization of PEFCs. Their focus has been on enhancing performance and reducing costs through innovative research and facilitating the commercialization of PEFC technology in the foreseeable future [19]. Table 2 provides a historical view on the evolution of fuel cell technology.

**Table 2:** Important Steps in the Aging and Implementation of PEFC [21].

| YEAR | PEMFC Technology | PEMFC Application |
|---|---|---|
| **1839** | First fuel cell | |
| **1955** | PEFC invention | |
| **1963** | | First practical fuel cell for the Gemini space mission |
| **1964** | First platinum-group-metal-free (PGM-free) catalyst | |
| **1966** | Nafion invention | |
| **1967** | First PEM electrolyzer | |
| **1987** | Dow membrane invention | |
| **1989** | Introduction of metal-nitrogen-carbon (M-N-C) catalyst | |
| **1995** | | Testing of PEFC on buses in Vancouver and Chicago |
| **2002** | | First commercial fuel-cell vehicle by Toyota |
| **2003** | | The first application of PEFC vehicle by Toyota |
| **2005** | | 6-hour rally by PEMFC-driven vehicles |
| **2008** | | First PEFC-driven ship |
| **2009** | | First large-scale residential program using PEFC in Japan |
| **2014** | | Toyota Mirai debut |

### 1.2.1 STRUCTURE OF POLYMER ELECTROLYTE FUEL CELLS

A single PEFC unit consists of several key components. The outer layers of the PEFC consist of a current collector with an embedded graphite plate on each side. Moving inward, we encounter the Gas Diffusion Layer (GDL), also called the Porous Transport Layer (PTL).

The GDL transports the reactants and products to and from the catalyst layers (CL), in which the electrochemical reaction takes place. At the center of the single PEFC lies the polymer electrolyte membrane (PEM). The PEM, catalyst layers, GDLs, and gaskets are usually combined and called the membrane electrode assembly (MEA) as shown in Figure 2.

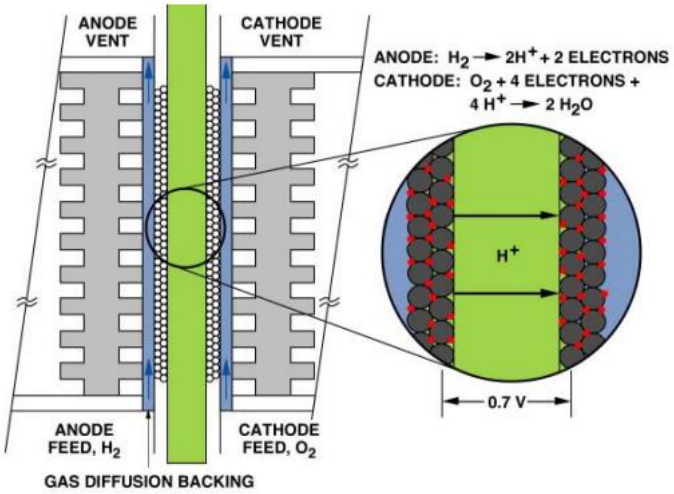


**Figure 2** MEA in a PEFC [22].

To prevent electron conduction within the cell and ensure proper sealing, the different components shown in Figure 3 are securely sealed with a gasket.

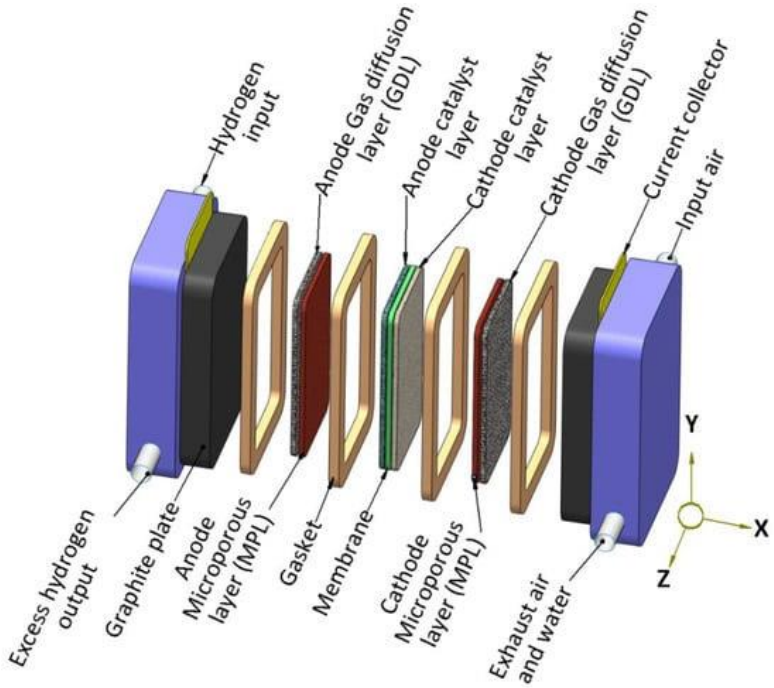


**Figure 3** Schematic of a PEFC [21].

#### 1.2.1.1 CURRENT COLLECTOR PLATES

The current collector plates (CCPs) play a vital role as the electrical terminals in a fuel cell unit. The CCP is often designed with an integrated flow field path, allowing reactants to flow along one side of its surface. This configuration enables the CCP to function independently as either the anode or cathode. Furthermore, the CCP serves multiple functions such as electrically connecting adjacent cells, providing structural support for the delicate membrane electrode assembly, facilitating water management within the cell, and sometimes serving as cooling plates for heat management [23].

#### 1.2.1.2 FLOW FIELDS

Flow fields play a key role in the distribution of fuel (hydrogen) and oxidant (air) to the anode and cathode electrodes, respectively, while also collecting electrons produced and removing water. Their design influences gas distribution, reactant utilization, and water management, crucial for optimizing fuel cell performance and efficiency.

#### 1.2.1.3 GAS DIFFUSION LAYERS

GDLs are commonly composed of carbon-based materials and are available in various forms, including cloth, non-woven pressed carbon fiber configurations, or a felt-like material. These GDLs are often treated with a hydrophobic material, such as polytetrafluoroethylene (PTFE). The inclusion of PTFE helps to create a hydrophobic surface that repels water from the membrane. This design feature is important for maintaining proper water management within the fuel cell system and preventing excessive water accumulation in the GDL, which could impede the electrochemical reactions and overall performance of the cell [7]. GDLs typically include a thinner microporous layer (MPL) that interfaces with the adjacent catalyst layer. This MPL facilitates electrical contact between the GDL and the catalyst layer while ensuring proper water transport [24].

#### 1.2.1.4 CATALYST LAYERS

CLs play a vital role in facilitating the electrochemical reactions within the PEFC. Typically, the PEFC electrode consists of a thin catalyst layer sandwiched between a porous electrically conductive substrate and the ionomer membrane. These electrodes are porous structures that contain a catalyst with high activity for the oxygen reduction reaction (ORR) at the cathode and the hydrogen oxidation reaction (HOR) at the anode. Platinum is the most

commonly used catalyst for both the ORR and HOR in PEFCs due to its exceptional performance and efficiency in these reactions [25].

#### 1.2.1.5 MEMBRANE

Currently, NAFION (Sodium (Na) and Fluorine (F) Ions) membranes are extensively utilized in PEFCs due to their favorable resistance to chemical attack from strong bases, oxidizing agents, and reducing agents. These membranes consist of a polymer backbone with attached sulphonic groups, which are crucial for enabling efficient proton conductivity. To ensure optimal proton transport, Nafion membranes require sufficient hydration. This hydration facilitates the movement of H+ ions as they jump from one sulphonic group to another, ultimately reaching the cathode side of the fuel cell. While these membranes allow hydrogen cations to permeate through, they effectively block the passage of oxygen anions [26].

### 1.2.2 WORKING PRINCIPLE OF PEFC

Typically, the PEFC is usually made up of layers, each with its own specific function. Figure 4 illustrates these layers, which include the anode plate, anode GDL, anode CL, PEM, cathode CL, cathode GDL, and cathode Plate.

At the anode of a running PEFC, the fuel is oxidized and a reduction reaction occurs at the cathode. Fuel (hydrogen) and oxygen (from air) are supplied to

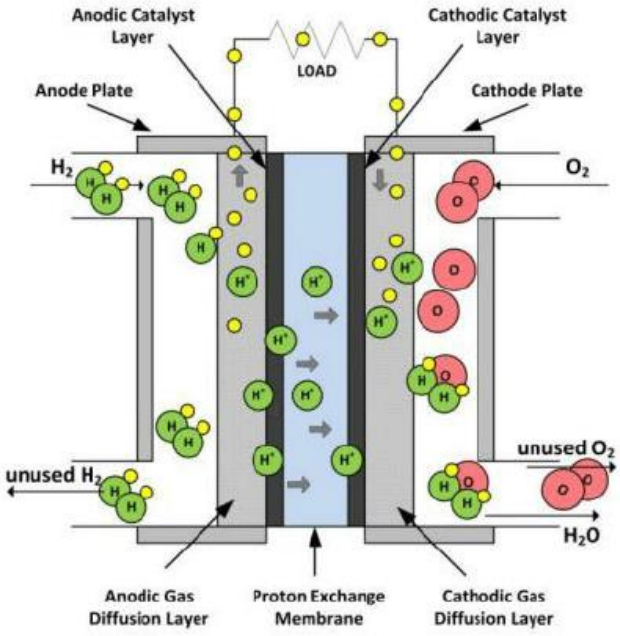


**Figure 4** PEFC Working Principle: Schematic Representation [27].

the system at the anode and cathode, respectively. At the anode side, hydrogen enters through the GDL and is oxidized when it reaches the anode CL,

$$2H_2 \longrightarrow 4H^+ + 4e^-.$$

This reaction is called Hydrogen Oxidation Reaction (HOR).

The PEM permits protons (along with water) to pass through to the cathode side while preventing the passage of electrons and gases. The electrons, repelled by the PEM, transit through the external electrical circuit, where the electric current can be utilized, before rejoining the cathode as shown in Figure 4.

In the presence of a catalyst on the cathode side, and with the protons transferred through the membrane and the electrons through the external circuit, the oxygen molecules ($O_2$) are reduced,

$$O_2 + 4H^+ + 4e^- \longrightarrow 2H_2O.$$

This reaction results from two reactions: the Oxygen Reduction Reaction (ORR),

$$O_2 + 4e^- \longrightarrow 2O^{2-},$$

and the reaction combining ionized species forming water as an end product,

$$2O^{2-} + 4H^+ \longrightarrow 2H_2O.$$

The global reaction at the cathode and anode is

$$2H_2 + O_2 \longrightarrow 2H_2O.$$

Water movement plays a crucial role in the functioning of the PEFC. As protons travel through the MEA, water is carried along by electro-osmotic drag, facilitating its movement to the cathode side. Conversely, a water concentration gradient leads to back diffusion, causing water to migrate from the cathode to the anode. Achieving optimal PEFC performance requires careful consideration of the interplay between these processes and the need to optimize every condition [28, 29]. Modifying a single parameter in the PEFC can trigger a chain reaction, affecting at least two other parameters and potentially yielding unexpected outcomes. Therefore, optimizing the operating conditions becomes imperative to maintain the desired operation [30].

### 1.2.3 DYNAMICS OF PEFC

The dynamics of a PEFC involve the complex interplay of various processes and phenomena including electrical, electrochemical, mass transport, and heat transfer, which contribute to its multi-physics nature:

- Electrochemical Double Layer (EDL): The EDL occurs at the interface between the electrode and the electrolyte, allowing charge transfer processes during the electrochemical reactions. The dynamic of the EDL is highly influenced by factors like potential, current density, water content, temperature, mass transport and catalyst activity. Changes in these parameters can affect the distribution of ions, thickness of the EDL, and charge transfer rate, impacting the fuel cell's overall performance.
- Mass Transport: Efficient mass transport of the reactants (hydrogen and oxygen) and products (water) is crucial for optimal PEFC operation. This involves the transport of gases through porous electrodes, diffusion of reactant gases to the catalyst sites, liquid water transport, water vaporization and removal of water vapor from the cathode.
- Liquid-vapor Exchange: This process depends on several factors including operating conditions, relative humidity, reactant flow rates, and temperature. The changes in temperature and humidity distribution during start-up or shut down of the cell affect the water phase distribution. When the temperature increases (start-up), it leads to an evaporation of livid water into vapor. The opposite scenario happens during shut down. Proper water management is required in order to avoid membrane drying.
- Heat Transfer: PEFCs generate heat as a byproduct during operation, which needs to be managed to maintain optimal performance and prevent overheating. Heat is produced due to the electrochemical reactions and resistive losses within the fuel cell. Effective heat transfer mechanisms, such as cooling systems or thermal management strategies, are employed to maintain the desired operating temperature.
- Water Management: PEFCs require careful control of water content within the cell. Water is produced at the cathode during the reaction and needs to be managed to prevent flooding or drying out of the membrane. Proper hydration of the membrane is essential for maintaining its conductivity and overall cell performance.

These phenomena have different time response characteristics (Figure 5). The fastest concerns the double layer capacity effects: occurring at the interface between the electrode (which allows the flow electrons) and the electrolyte (through which ions flow) within the fuel

cell. Then comes the transfer of charges due to the electrochemical reactions (oxidation and reduction), the gas diffusion through the channel or the GDL, occurring at timescale of few seconds, and the hydration of the membrane, which takes seconds or several minutes depending on the fuel cell's operating conditions. On the other hand, some processes happen slowly. For example, the electrodes can get affected by impurities in the reactants (usually carbon monoxide in very small amounts) or by the formation of an oxide layer over minutes to hours. There are also thermal changes that can happen within minutes or hours, influenced by factors like the materials used, gas flow rates, and ambient temperature. Lastly, over a long period of operation, structural changes can occur in the electrodes and electrolytes, leading to irreversible performance degradation [17].

Figure 5 illustrates the timescales involved in the operation of a PEFC, ranging from microseconds to years ($10^{-6}$ s to $10^{8}$ s). It shows that electrochemical reactions take place at the surface of catalytic nanoparticles, while gases are supplied through pipes of a few centimeters in size. A fuel cell is not only a system involving multi-physics, but also a temporally and

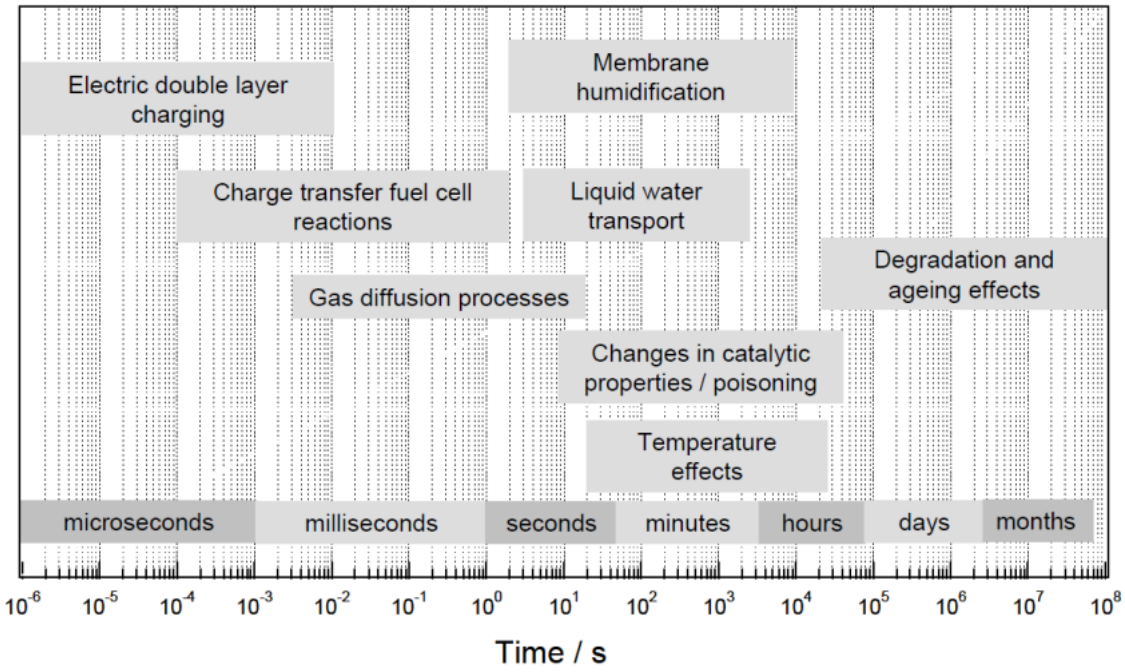


**Figure 5** Overview of dynamic processes in PEFC [17].

spatially multi-scale and coupled object. In other words, a fuel cell is a complex system, encompassing various interconnected aspects [17].

## 1.3 DIAGNOSTICS OF PEFC

The durability and reliability of PEFCs are important factors that impact their widespread use. PEFCs can encounter various issues or faults that result in performance losses and degradation. The main faults include flooding (too much water inside), drying (insufficient moisture), fuel or oxidant starvation (not enough hydrogen or oxygen), and catalyst poisoning (contamination of catalyst material) [31]. To avoid such obstacles, diagnostic techniques are highly valuable throughout the development, manufacturing, and operation of PEFCs, as they help detect and identify faults in real-time.

Diagnostic techniques primarily draw upon existing electrochemical techniques that have been adapted and tailored for the specific diagnostic needs of PEFCs. Through the application of these diagnostic methods, researchers and engineers can gain valuable insights into the performance, condition, and potential challenges encountered by PEFC systems. These techniques help in different ways: during development, they measure properties and processes to find limitations and optimize performance; in manufacturing, they ensure quality control with speed and accuracy; and during operation, they assess the condition of the fuel cell and provide vital information for its management. Diagnostic tools monitor variables like voltage, current, temperature, and concentration, and can evaluate fuel cell health, electrocatalytic activity, and faults. These tools are crucial for ensuring the reliability and efficiency of fuel cells at every stage [9].

## 1.4 OVERVIEW OF FREQUENCY RESPONSE ANALYSIS AS A DIAGNOSTIC TECHNIQUE

Frequency response analysis (FRA) techniques form a valuable class of techniques used to understand the behavior of dynamic systems. It finds applications in various fields and is used to characterize mechanical, electromagnetic, and electrochemical systems. By applying FRA, parameters of these systems can be identified and analyzed. Moreover, FRA is particularly effective in detecting abnormal operating conditions in electric motors, making it a useful tool in motor diagnostics and fault detection [32].

FRA techniques involve applying periodic disturbances to the system under investigation as shown in Figure 6 by varying the frequency of an input variable.

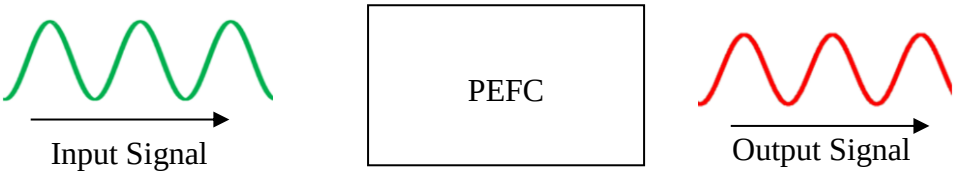


**Figure 6** Schematic diagram of FRA for a PEFC system.

The system's response is then analyzed using the Fourier Transform. It's important to use small amplitudes for the input disturbances to ensure a linear response from the system. By examining the resulting response across a range of input frequencies, the system is sequentially subjected to disturbances that affect processes with various time constants. This allows for the examination of how the system responds differently to these perturbations at different frequencies. It helps in understanding the dynamics and time-dependent behaviors of the system under investigation.

As mentioned in the introduction section, in FRA electrical perturbation signals, such as current and voltage, are often associated with impedance-based techniques like Electrochemical Impedance Spectroscopy (EIS). These techniques involve analyzing the system's response to small amplitude sinusoidal perturbations applied at different frequencies. They provide valuable information about the system's impedance and can help identify electrochemical processes, charge transfer resistances, and transport parameters. Similarly, it is also possible to use other perturbation signals like pressure, concentration, humidity, or temperature, for the development of corresponding diagnostic techniques. These may include Electrochemical Pressure Impedance Spectroscopy (EPIS), Concentration Admittance Spectroscopy (CAS), Species Frequency Response Analysis (sFRA), or Concentration-alternating Frequency Response Analysis (cFRA). By employing these techniques, a comprehensive set of diagnostic tools can be devised to comprehensively assess and analyze the behavior and performance of the system under investigation [9].

Table 3 presents a comprehensive list of input and output combinations used in the FRA techniques applied to PEFCs.

**Table 3:** An overview of input/output combinations applied in PEFC research and corresponding frequency response functions (adopted and extended from [10]).

| Input / Output | $I$ | $V$ | $P_{out}$ | $P_{O_2}$ | $P_{H_2O}$ | $T_{cell}$ | $T_{sur}$ | $t_{H_2O}$ | $c_{O_2}$ |
|---|---|---|---|---|---|---|---|---|---|
| $I$ | $X$ | $EIS$ | $EPIS$ | $cFRA(O_2)$ | $cFRA(H_2O)$ | | | | |
| $V$ | $EIS$ | $X$ | $EPIS$ | $cFRA(O_2)$ | $cFRA(H_2O)$ | | | | |
| $P_{out}$ | $EPIS$ | $EPIS$ | $X$ | | | | | | |
| $P_{O_2}$ | | | | $X$ | | | | | |
| $P_{H_2O}$ | | | | | $X$ | | | | |
| $T_{cell}$ | | | | | | $X$ | | | |
| $T_{sur}$ | $ETIS$ | | | | | $LIT$ | $X$ | | |
| $t_{H_2O}$ | $HECII$ | | | | | | | $X$ | |
| $c_{O_2}$ | $CAS$ | | | | | | | | $X$ |

## 1.5 ELECTROCHEMICAL IMPEDANCE SPECTROSCOPY

In the last decades, EIS has emerged as a powerful and extensively used tool for studying electrochemical systems. It has gained popularity as the most widely employed method in this field. One of the key objectives of using EIS in electrochemistry is to gain a deeper understanding of the mechanisms underlying reactions and transport phenomena within a system. This includes studying processes such as the flow of chemical species, current flow, mass transport, corrosion rates, and deposition rates. By investigating these factors, it becomes possible to evaluate system-specific parameters. These parameters, such as kinetic coefficients, diffusion coefficients, surface concentrations of adsorbed intermediates, and viscosity coefficients, provide valuable insights into the fundamental characteristics and behavior of the system. Through the analysis of these parameters, researchers can enhance their understanding of the complex processes occurring within electrochemical systems.

EIS enables comprehensive analysis of the electrical response of a system over a range of frequencies (usually from 1 mHz to 100 kHz). By applying an alternating current (AC) voltage or current to an electrode, and measuring the resulting current or voltage, valuable

insights into the electrochemical processes [33], charge transfer resistances, and diffusion limitations [34, 35] can be obtained. Unlike direct current (DC) measurements that focus on resistance (R), EIS expresses the relationship between voltage and current as impedance (Z) which essentially refers to how well a system resists the flow of electrical current. It quantifies the system's ability to impede or hinder the movement of electrical charges [36].

EIS is typically performed using a small excitation signal in order to ensure linear response from the cell. This means that the output signal of the system is linearly related to the input signal (if a sinusoidal potential is applied, the resulting current response also becomes a sinusoid at the same frequency but with a phase shift and different amplitude). The potential ($E$), current ($I$), and the corresponding impedance ($Z$) can be described as the following, respectively [37]:

$$E(t) = |E| \exp(j\omega t), \quad 1\text{-}1$$

$$I(t) = |I| \exp(j\omega t + j\varphi), \quad 1\text{-}2$$

$$Z(\omega) = \frac{E(t)}{I(t)} = |Z| exp(-j\varphi), \quad 1\text{-}3$$

with $\omega = 2\pi f$, the angular frequency, $f$ the frequency, $j$ the imaginary unit, $t$ the time, and $\varphi$ the phase shift.

This can be assessed by fitting a PEMFC model to the EIS spectra. Three commonly used model approaches are typically employed for this purpose: (i) physics-based models, (ii) equivalent circuits (EC), and (iii) data-driven models. Physics-based models are built on fundamental physical principles and mathematical representations, while equivalent circuits represent the different reactions involved in the system using lumped electrical components. Data-driven models, on the other hand, rely on statistical techniques to extract patterns and relationships from experimental data [10].

The versatility and effectiveness of EIS have made it a go-to technique for researchers and engineers studying various electrochemical systems [38].

Impedance spectra are commonly represented using both Bode and Nyquist plots which can offer comprehensive understanding of the impedance behavior. Figure 7 illustrates both of these representations.

### 1.5.1 NYQUIST PLOT

The Nyquist plot is commonly used to represent the impedance spectrum. It consists of a graph where the negative imaginary part of the impedance is plotted against the real part. Typically, the plot exhibits two or more semicircles at different frequency ranges. The size and

shape of the semicircles provide valuable information about the system's electrical behavior and characteristics [39].

### 1.5.2 BODE PLOT

While the Nyquist plot is widely used in EIS measurements, other representations such as Bode magnitude (magnitude vs. frequency) and phase (phase vs. frequency) plots have been utilized to extract additional information not readily obtained from the Nyquist plot. These alternative plots have the advantage of highlighting local maximum values in the Bode phase plot, which correspond to characteristic frequencies inversely proportional to the time constants of the underlying processes [39].

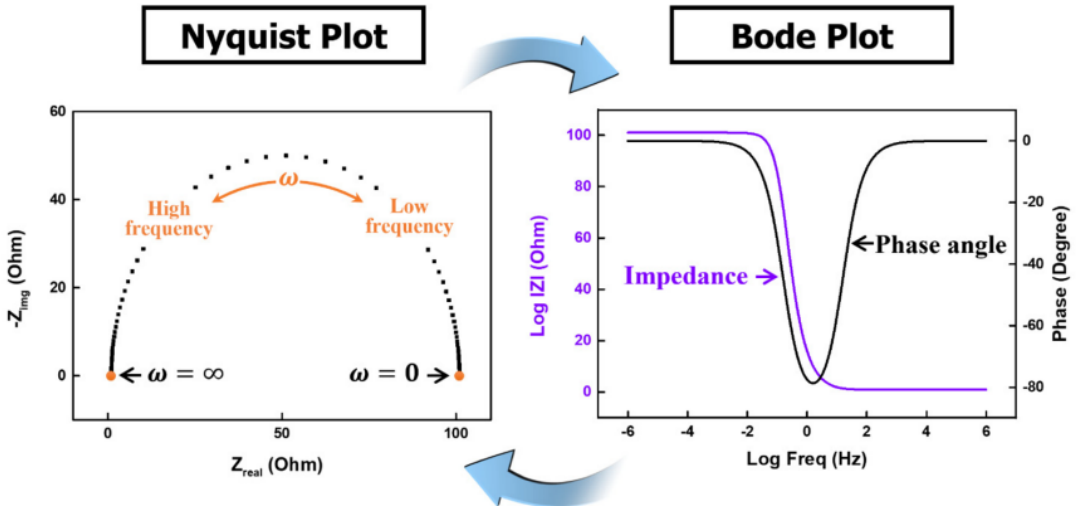


**Figure 7** EIS representation by Nyquist plot (left) and Bode plot (right) [40].

## 1.6 CONCENTRATION-ALTERNATING FREQUENCY RESPONSE ANALYSIS

Sorrentino et al. [41] recently introduced a new FRA technique called concentration-alternating frequency response analysis (cFRA). In the cFRA technique, a periodic variation in the concentration of a reactant or product is introduced as an input. Depending on the experimental conditions, the most appropriate electrical output variable, such as current or potential, is chosen for analysis. This technique utilizes transfer functions that depend on perturbations of specific reactant partial pressures. Their theoretical work demonstrated that cFRA spectra can distinguish between different dynamic processes occurring in the cell based on the type of concentration perturbation (such as oxygen or water partial pressure) and the applied electrical control (such as voltastatic or galvanostatic).

In a separate publication by Sorrentino et al. [10], they conducted initial experiments using the cFRA technique on a laboratory-scale PEFC. The analysis of the obtained transfer

functions revealed valuable insights into gas and water transport within different layers of the cell. Furthermore, the study demonstrated the capability of the cFRA method to diagnose issues associated with the cathode's humidification condition.

Studies have demonstrated that cFRA spectra possess the ability to distinguish various dynamic processes occurring within a fuel cell, depending on the type of concentration perturbation and the applied electric control. For instance, when employing galvanostatic cFRA with oxygen perturbations, it becomes possible to selectively detect gas transport dynamics within the channel. Comparing cFRA spectra obtained under voltastatic and galvanostatic controls for oxygen perturbations enables the identification of water transport contributions in the membrane's dynamics. Additionally, these phenomena can be selectively studied through cFRA transfer functions based on water pressure perturbation. By utilizing partial pressure perturbations, a more accurate estimation of kinetic and transport parameters can be achieved compared to traditional EIS. Among the various diagnostic tools, cFRA performed using water pressure inputs has shown the most promising performance, particularly for onboard applications [41].

These findings highlight the potential of the cFRA technique as a diagnostic tool for understanding and addressing challenges related to gas and water management in PEFCs.

## 1.7 ELECTROCHEMICAL PRESSURE IMPEDANCE SPECTROSCOPY

In 2010, Niroumand et al. [42] introduced a novel approach that utilizes the ratio of voltage to pressure amplitude and the phase shift between the voltage response and pressure perturbation signal for the extraction of diagnostic information about the fuel cell cathode. In their study, they observed periodic fluctuations in the cell voltage of the PEFC. Interestingly, these fluctuations occurred at the same frequency as the fluctuations in the cathode output pressure, which was approximately 0.14 Hz [42]. This observation suggests a direct correlation between the pressure variations in the cathode and the resulting voltage fluctuations in the fuel cell. These findings led to the concept of incorporating pressure as a dynamic state variable in addition to current and voltage in frequency response analysis experiments, which expanded perspective acknowledges the significance of pressure dynamics and highlights its potential role in understanding the behavior and performance of the fuel cell system.

In 2014, Hartmann et al. [43] introduced the concept of Electrochemical Pressure Impedance Spectroscopy (EPIS) as a technique to investigate the dynamic behavior of pressure alongside electric state variables within the frequency domain. An advantage of EPIS is that its

spectra, focus solely on non-faradaic processes. These spectra predominantly reflect oxygen and water transport phenomena in the cell cathode, particularly in the frequency range below 100 Hz. This characteristic makes EPIS a valuable complementary technique to EIS [44].

In 2016, Engebretsen et al. [45] conducted the first experimental application of EPIS in a PEMFC. Their experimental setup involved modulating the cathode backpressure by applying a sinusoidal current to a speaker using a potentiostat. The resulting pressure "front" at the fuel cell had an amplitude of 60 Pa within the investigated frequency range and analyzed the voltage response. The combination of current, voltage, and pressure dynamics in EPIS enables the exploration of various representations beyond the standard $Z_p = Z_{P/Q} = p(t)/Q(t)$, where $Q$ is the electrical charge and $p$ the pressure. Additional representations such as $Z_{P/I} = p(t)/I(t)$ or $Z_{E/P} = E(t)/p(t)$ can be achieved by varying either the voltage or the chamber pressure [43]. These alternative representations offer different perspectives and insights into the interplay between pressure, current, and voltage within the system. By manipulating these variables, researchers can gain a more comprehensive understanding of the complex dynamics and interactions within PEFC.

## 1.8 CONCENTRATION ADMITTANCE SPECTROSCOPY

In their recent work, Sun et al. [13] have reported a diagnostic technique named Concentration Admittance Spectroscopy (CAS) which includes perturbing the system with a small-amplitude modulation in electrode potential and measuring the corresponding response in oxygen concentration, offering valuable complementary capabilities for studying and analyzing oxygen transport processes. CAS offers a unique advantage as it does not rely on external perturbation of pressure or concentration. Instead, it involves measuring the oxygen concentration at the outlet of the cathode channel during a standard EIS measurement [13].

By focusing on the measurement and analysis of oxygen concentration dynamics, CAS provides additional insights into the intricate mechanisms and behaviors associated with oxygen transport in the system. Sun et al. [13] showcase how valuable information regarding the oxygen transport coefficients in different components, including the flow field channel, gas diffusion layer, and catalyst layer, can be extracted from the admittance measurements at the air channel outlet. This knowledge is crucial for understanding and optimizing the oxygen transport processes, which ultimately impact the overall performance and efficiency of the system.

## PARTIAL CONCLUSION

There are different types of fuel cells, categorized based on their operational temperature or the nature of their electrolyte. Currently, the Polymer Electrolyte Fuel Cell (PEFC) stands out as the most extensively studied technology, due to its numerous advantages such as high efficiency, low operating temperature, and environmental friendliness, etc. Nevertheless, to ensure reliable operation, and optimal performance of PEFC, the use of accurate diagnostic techniques is essential.

Frequency Response Analysis (FRA) techniques, including methods like EIS, EPIS, cFRA, CAS have proven to be valuable tools for evaluating PEFC. These techniques provide in-depth insights into the fuel cell's behavior by applying a small amplitude of an input and analyzing the output signal.

# CHAPTER 2:
# MODELING AND ANALYSIS

# CHAPTER 2: MODELING AND ANALYSIS

In this chapter, we will explain how we built and studied our research models. The chapter lays the foundation for our study, outlining the step-by-step methods we used to investigate our topic.

## 2.1 MODELING

EIS has the merits of being a non-invasive technique that involves exciting the electrochemical system with a small sinusoidal potential or current signal to measure its linear response across a broad frequency range [46]. EIS is used for in situ measurements of transport and kinetic properties in the functional layers of PEFCs. Unlike static methods, EIS uses the dynamic behavior to separate contributions from different processes within the total voltage loss of the cell. This makes it an incredibly powerful and appealing tool for both the design and testing of fuel cells. EIS provides visibility to all transport and kinetic processes in a fuel cell since they are ultimately connected to the transport and conversion of charges. However, in order to interpret impedance spectra accurately, modeling techniques are necessary [47]. Physics-based modeling and equivalent circuit modeling are the two approaches considered in this work.

### 2.1.1 SIMPLE PEFC MODEL

#### 2.1.1.1 PHYSICAL MODEL

Physics-based modeling refers to the mathematical representation of the system based on the underlying physical principles that govern the system's behavior. In the last years, following early work by Eikerling and Kornyshev [34], there has been a noticeable shift in the literature [48–52] towards physics-based impedance models, moving away from simple equivalent circuits.

The cathode catalyst layer (CCL) is one of the significant elements within a PEMFC as most of the losses occur here. Kulikovsky and Eikerling [15] have reported a physical model impedance of the CCL based on the governing equations describing the CCL performance [53, 54],

$$C_{dl}\frac{\partial \eta}{\partial t}+\frac{\partial j}{\partial x}=-2i_{*}\left(\frac{c}{c_{ref}}\right)sinh\left(\frac{\eta}{b}\right), \qquad 2\text{-}1$$

$$j=-\sigma_{p}\frac{\partial \eta}{\partial x}, \qquad 2\text{-}2$$

where $C_{dl}$ is the double layer volumetric capacitance (F cm$^{-3}$), $\eta$ is the half-cell overpotential, $t$ is time, $j$ is the local proton current density, $x$ is the distance from the membrane, $i_*$ is the volumetric exchange current density (A cm$^{-3}$), $c$ oxygen concentration in the CCL (here assumed to be independent of $x$), $c_{ref}$ is the reference oxygen concentration, $\sigma_p$ is the proton conductivity, $b$ is the Tafel slope,

$$b = \frac{RT}{\alpha F}, \qquad 2\text{-}3$$

where $\alpha$ is the transfer coefficient, $R$ is the gas constant, $F$ the Faraday constant, and $T$ is the temperature.

Dimensionless variables were introduced in order to simplify calculations:

$$\tilde{x} = \frac{x}{l_t}, \tilde{t} = \frac{t}{t_*}, \tilde{\eta} = \frac{\eta}{b}, \tilde{j} = \frac{j}{j_*}, \tilde{Z} = \frac{Z\sigma_p}{l_t}, \tilde{c} = \frac{c}{c_{ref}}; \qquad 2\text{-}4$$

where $l_t$ is the CCL thickness and

$$t_* = \frac{C_{dl}b}{2i_*}, j_* = \frac{\sigma_p b}{l_t}, \qquad 2\text{-}5$$

are the scaling parameters for time and current density, respectively. With these variables, the system (2-1) and (2-2) takes the form:

$$\frac{\partial\tilde{\eta}}{\partial\tilde{t}} + \varepsilon^2\frac{\partial\tilde{j}}{\partial\tilde{x}} = -\tilde{c}\,sinh\,\tilde{\eta}, \qquad 2\text{-}6$$

$$\tilde{j} = -\frac{\partial\tilde{\eta}}{\partial\tilde{x}}, \qquad 2\text{-}7$$

where,

$$\varepsilon = \sqrt{\frac{\sigma_p b}{2i_* l_t^2}}, \qquad 2\text{-}8$$

is the dimensionless reaction penetration depth.

Based on these equations, an analytical solution for the impedance response of the CCL was reported in [15], which considers the low current densities regime of CCL operation, where oxygen transport losses can be ignored. Therefore, the oxygen concentration in the CCL is considered as constant. With the definition of the impedance,

$$\tilde{Z} = \frac{\tilde{\eta}^1}{\tilde{j}^1}, \qquad 2\text{-}9$$

where $\tilde{\eta}^1$ and $\tilde{j}^1$ are respectively the perturbation of the total voltage loss in the system and the perturbation of proton current density at $\tilde{x} = 0$ (membrane/CCL interface), the impedance of the CCL is given as,

$$\tilde{Z} = -\frac{1}{\varphi\tan\varphi}, \qquad 2\text{-}10$$

with,

$$\varphi = \sqrt{-\frac{\beta^2}{2} - ip}, \qquad 2\text{-}11$$

$$p = \frac{\widetilde{\omega}}{\varepsilon^2}, \qquad 2\text{-}12$$

$$\beta = \sqrt{2\tilde{j}_0^0}, \qquad 2\text{-}13$$

where $\widetilde{\omega} = \omega * t_*$, $\omega$ is the angular frequency and $\tilde{j}_0^0$ is the dimensionless steady-state proton current density at the membrane/CCL interface. In this thesis work, this model is used to characterize controllability, observability and sensitivity as discussed in the introduction and section 2.2.

### 2.1.1.2 EQUIVALENT CIRCUIT MODEL

Equivalent circuit models (ECM) have been proposed for EIS analysis due to their simplicity and versatility to describe a broad range of operating conditions [10]. Research has shown that the electrode/electrolyte interface can be effectively represented using an equivalent circuit (EC) (as illustrated in Figure 8), comprising different impedance elements, including resistor, capacitance, and Warburg element, to name a few [55] that represent the various reaction steps involved [56]. The way these impedance elements are connected depends on how the processes they represent are related. If the steps happen one after the other, they are connected in a series. If they happen simultaneously, they are connected in parallel [57]. The EC technique is easy to implement and understand for impedance spectra analysis.

Figure 8 consists of an equivalent circuit (a) and a Nyquist plot (b). The EC consists of several components, including a charge transfer resistance ($R_{ct}$) that represents the electron transfer in the electrochemical reaction at the electrode, a resistance $R_m$

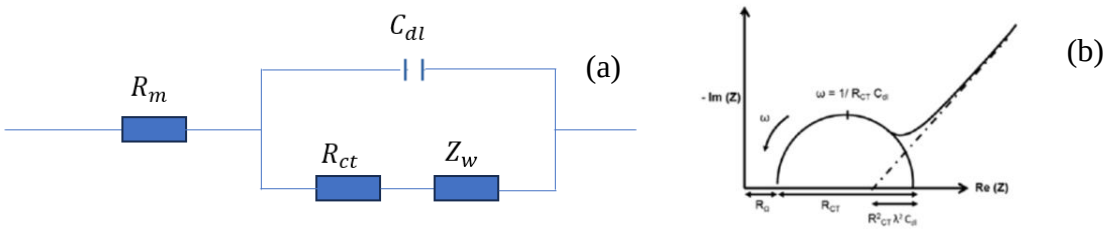


**Figure 8** (a) Randles equivalent circuit, and its (b) characteristic Nyquist plot for impedance modeling of the cell cathode.

for the membrane and contact resistances, a double-layer capacitor ($C_{dl}$), and a diffusion convection impedance ($Z_w$).

Several configurations of EC have been reported in the literature [58–65]. EC techniques have been widely applied in modeling and characterizing diverse phenomenological processes within PEFCs. Researchers have frequently employed Randles circuits, without the Warburg element, which typically describes the finite diffusion processes of chemical species, connected in series with a resistance to construct the EC for PEFC impedance obtained through EIS analysis [65]. Alternatively, other researchers utilize this Randles circuit with the addition of a Warburg element (Figure 8) to account for oxygen transport limitations at high currents during EIS measurements [60, 63]. However, research has shown that Randles circuits have their limitations. In a work done by Touhami et al. [66] it is reported that these circuits do not consider the high frequency straight line, which is associated with proton transport in the CCL. The use of a transmission line model was introduced in earlier works: investigations involving EIS on porous electrodes were conducted by De Levie, where he presented the transmission line model (TLM) (see Figure 9) [57]. This model describes the pores of a porous electrode as essentially circular cylindrical channels with a uniform diameter and infinite length [57].

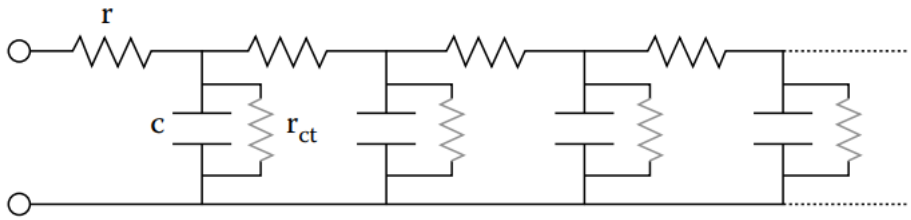


**Figure 9** TLM proposed by De Levie [57].

In the same line, Eikerling and Kornyshev [62] have reported a TLM to represent the impedance and to characterize the porous CL of PEMFC in the absence of oxygen transport limitations in the CCL. Makharia et al. [64] followed up with a TLM neglecting oxygen transport limitations and compared the results with the results of Eikerling and Kornyshev [62] for low currents. Furthermore, a TLM was derived by Cruz-Manzo and Chen [55] to describe intermediate and high currents, incorporating a Warburg element to consider oxygen diffusion, and a charge transfer resistance in parallel with a constant phase element to account for the kinetics of the ORR.

In a recent study by Kulikovsky [47], based on the performance of the CCL described by the charge conservation, Ohm's law, and mass conservation equations, an analytical solution for the impedance response of the CCL was derived. In this report, a TLM is constructed to

calculate the impedance response of the CCL taking into account oxygen transport and compared with the physical result of Kulikovsky [47].

## 2.2 ANALYSIS

### 2.2.1 SENSITIVITY ANALYSIS

Sensitivity analysis is a widely used technique to examine how changes in model parameters, such as operating conditions, cell or materials parameters, affect the desired outputs [67]. It assists in identifying the key parameters that greatly influence the model's output, providing valuable insights into the system's behavior. In the fuel cell literature, sensitivity analysis typically involves individually perturbing the parameter of interest to evaluate the significance of each parameter [68, 69].

In this regard, relative sensitivities were introduced as a measure to evaluate the effectiveness of different methods [11–13]. By utilizing relative sensitivities, the strength and performance of various approaches can be assessed and compared. To examine the impact of parameters on a model using relative sensitivity measure denoted $S_R$, Sun et al. [13] have suggested the following:

$$S_R = \frac{\delta|Y|/|Y|}{\delta\theta/\theta}, \qquad 2\text{-}14$$

where $\delta\theta$ represents the absolute value of the variation in the parameter $\theta$, $|Y|$ denotes the magnitude of the corresponding electrochemical impedance or concentration admittance at the initial value of $\theta$, and $\delta|Y|$ represents the change in magnitude of the electrochemical impedance or concentration admittance (i.e., $\delta|Y| = |Y_{\theta+\delta\theta}| - |Y_{\theta}|$). This definition offers several advantages. Firstly, it enables a comparison between different methods, even if they have values in different units and orders of magnitude. Secondly, it focuses solely on the model, disregarding any potential influence of measurement inaccuracies [13].

### 2.2.2 LINEAR SYSTEMS THEORY: CONTROLLABILITY AND OBSERVABILITY

Observability and controllability are fundamental concepts in linear systems theory that assess the ability to fully observe the internal state of a system and control it, respectively. The pioneering work on these concepts was initiated by R. Kalman in 1960 [70].

- Observability refers to the property of a system that allows its internal states to be determined or observed from the available system outputs. An observable system provides sufficient information about its internal states through its output

measurements. In other words, given enough input and output data, the system's internal states can be reconstructed accurately [71].

- Controllability refers to the property of a system that allows its internal states to be manipulated or steered to a desired state using suitable control inputs. A controllable system can be driven from any initial state to any desired state within a finite time by choosing appropriate control inputs [71].

A general mathematical framework based on linear system theory was established by Sorrentino et al.[10]:

$$\frac{dX}{dt} = F(X, U), \qquad 2\text{-}15$$

$$Y = G(X, U). \qquad 2\text{-}16$$

The vector $X$ contains the state variables (represented by $x_i$), which describe the state of the system as shown in Figure 10. The vector $U$ contains input quantities or constraints (represented by $u_j$) imposed by the experimental conditions. The vector $Y$ contains output variables (represented by $y_k$) that allow us to observe the system's state. In most cases, the

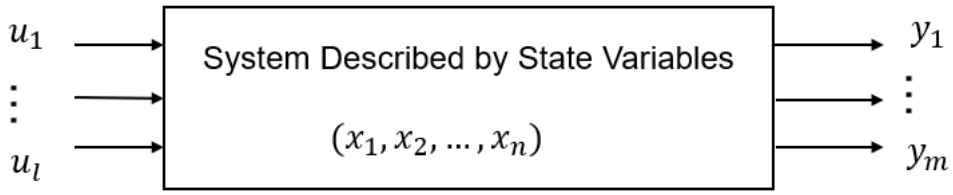


**Figure 10** Diagram description of a system.

functions $F_i$ and $G_k$ are nonlinear as most of the physical systems are. For distributed systems, the partial differential equations can be converted into a system of ordinary differential equations using numerical methods for discretization.

In the context of electrochemical systems, the elements of these vectors can represent various properties. For instance, $x_i$ may refer to reactant concentrations, coverage fraction of species on the electrode surface, or local overpotential. The elements of $u_j$ can encompass overall voltage or current, temperature, pressure, inlet concentration, flow rate, and more. As for $y_k$, it can include measured quantities such as voltage, current, reflective power, mass changes due to adsorption/desorption, and outlet reactant or product concentrations.

The nonlinearities in the functions $F_i$ and $G_k$ are often due to the exponential activation of electrochemical reaction rates by the potential. When examining the system at a fixed steady

state, the response to a small input perturbation can be calculated by linearizing the equation system around the steady state values of the variables. This process yields a simplified version of the system:

$$\frac{dX}{dt} = AX + BU, \qquad 2\text{-}17$$

$$Y = CX + DU. \qquad 2\text{-}18$$

The matrices A, B, C, and D, known as the state space, controllability, observability, and transmission matrices, respectively, consist of components that are defined as follows:

$$A_{i,j} = \frac{\partial F_i}{\partial x_j}|_{x_k,u_m,k\neq j}, \quad B_{i,j} = \frac{\partial F_i}{\partial u_j}|_{x_k,u_m,m\neq j}, \quad C_{i,j} = \frac{\partial G_i}{\partial x_j}|_{x_k,u_m,k\neq j}, \quad D_{i,j} = \frac{\partial G_i}{\partial u_j}|_{x_k,u_m,m\neq j}. \qquad 2\text{-}19$$

It is important to note that the elements of matrix A are influenced by the inherent dynamic characteristics of the system. On the other hand, the elements of matrices B and C are determined by the specific type of input and output being considered.

In general, the system's response to a perturbation is described by the transfer function $H(i\omega)$ in the frequency domain. The transfer function is obtained by applying the Fourier transform to the system of Equations (2-17) and (2-18). It can be represented as

$$H(i\omega) = \frac{\tilde{Y}(i\omega)}{\tilde{U}(i\omega)} = C(i\omega I_n - A)^{-1}B + D. \qquad 2\text{-}20$$

Considering $\Lambda$ as a diagonal matrix ($\Lambda = diag(\lambda_i) \quad (i = 1,2 \dots n)$) where $\lambda_i$ represents the eigenvalues of matrix $A$, and $P$ as the matrix of the corresponding left eigenvectors ($p_i$), and $Q^T = P^{-1}$ as the matrix of the corresponding right eigenvector ($q_i^T$), the equivalent canonical form of the system described by Equations (2-17) and (2-18) can be expressed as:

$$\frac{dX_d}{dt} = \Lambda X_d + Q^T BU = X_d + \beta U, \qquad 2\text{-}21$$

$$Y = CPX_d + DU = \gamma X_d + DU. \qquad 2\text{-}22$$

In this new representation, the matrix $\beta = Q^T B$ represents the normal form of the input matrix, and $\gamma = CP$ represents the normal output matrix. With this representation, the transfer function described in Equation (2-20) for a single input single output (SISO) system can be simplified and expressed as follows:

$$H(i\omega) = CP(i\omega I_n - \Lambda)^{-1}Q^T B + D = \sum_{k=1}^{n} \frac{r_k}{i\omega - \lambda_k} + d_1, \qquad 2\text{-}23$$

where,

$$r_k = Cp_k q_k^T B = \sum_{i=1}^{n}\sum_{j=1}^{n} c_{1,i}p_{i,k}q_{k,j}^T b_{j,1} = \gamma_{1,k}\beta_{k,1}. \qquad 2\text{-}24$$

The quantities $r_k$ represent the elements of the residual vector, each associated with a specific dynamic state variable $k$ characterized by a time constant $\tau_k = -\frac{1}{\lambda_k}$. As shown, these values depend on the product of the $k$ elements of the normal form of the input and output vectors, determining the contribution of the corresponding state variable $k$ in the transfer function for a given input/output system description. If one of the elements of $\gamma$ is zero or significantly smaller compared to the others, it indicates that the dynamics related to the $k$ variable cannot be observed or does not make a substantial contribution to the transfer function based on the considered output. Similarly, if one of the elements of $\beta$ is negligible or zero relative to the others, it implies that the corresponding $k$ variable is not controllable and has no influence on the transfer function derived using the related input.

## PARTIAL CONCLUSION

Different FRA techniques are highlighted in the literature review chapter, with EIS being the most widely employed. EIS involves perturbing the system with a small sinusoidal potential or current and then analyzing the impedance response. However, to accurately interpret the impedance spectra, modeling techniques are indispensable.

In our research, we consider two modeling approaches: physics-based modeling and equivalent circuit modeling. To conduct our analysis, we utilize a mathematical framework based on linear system theory, as developed in a previous study. This framework enables us to characterize controllability and observability using an existing analytical solution. Additionally, for sensitivity analysis, we employ the formula of relative sensitivity, which helps us evaluate how the model is sensitive to variations in a particular parameter.

# CHAPTER 3:

# RESULTS AND DISCUSSION

# CHAPTER 3: RESULTS AND DISCUSSION

In this following chapter, we will present the findings of our research and engage in a detailed conversation about their significance within the context of our study. This chapter serves as a platform of presenting and analyzing the outcomes of our research.

## 3.1 SIMPLE PEFC MODEL

### 3.1.1 ANALYTICAL MODEL

The analytical model derived by Kulikovsky and Eikerling [15] is employed in this section. Equation 2-10 can be simulated (see Figure 11) using the parameters in Table 4.

**Table 4:** Physical Parameters [15].

| | |
|---|---|
| Tafel slope $b$ , V | 0.05 |
| Proton conductivity $\sigma_p$ , $\Omega^{-1}$ cm$^{-1}$ | 0.03 |
| Exchange current density $i_*$ , A cm$^{-3}$ | $10^{-3}$ |
| CL capacitance $C_{dl}$ , F cm$^{-3}$ | 20 |
| CL thickness $l_t$ , cm | 0.001 |
| $j_*$ , A cm$^{-2}$ | 1.5 |
| $t_*$ , s | 500 |
| $\varepsilon^2$ | $7.5 * 10^5$ |
| $\tilde{j}_0^0$ | 0.1 |

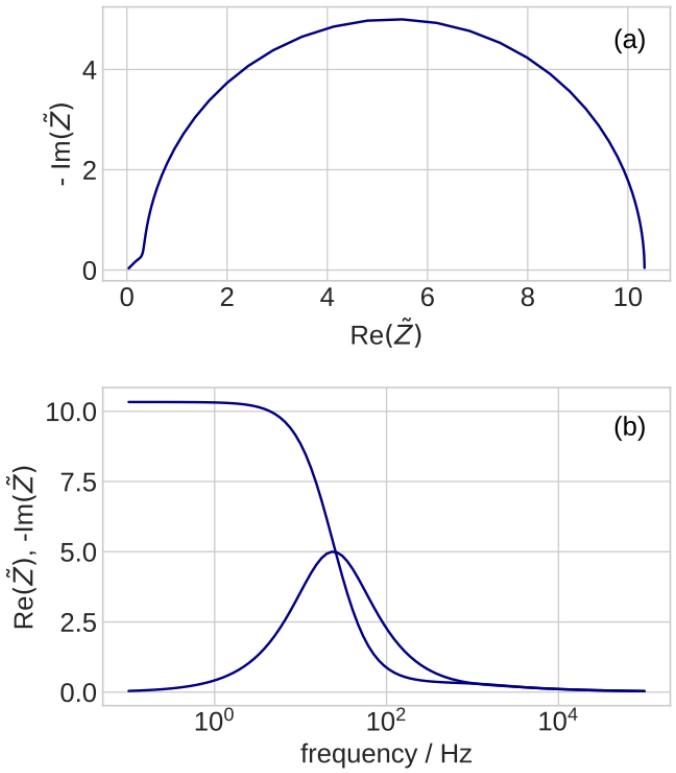


**Figure 11** (a) Nyquist spectrum and (b) Frequency dependance of the Nyquist spectrum of Eq. 2-10 with the parameters of Table 4.

In our work, a TLM is used to calculate the impedance of the CCL using the same assumptions. In this model, the CCL is segmented into $N$ slices ($N = 100$) and each element is represented by a RC-circuit of the protonic resistivity in series with the charge transfer resistivity which is parallel with the double layer capacitor. The $N$ elements are connected in parallel as showed in Figure 12.

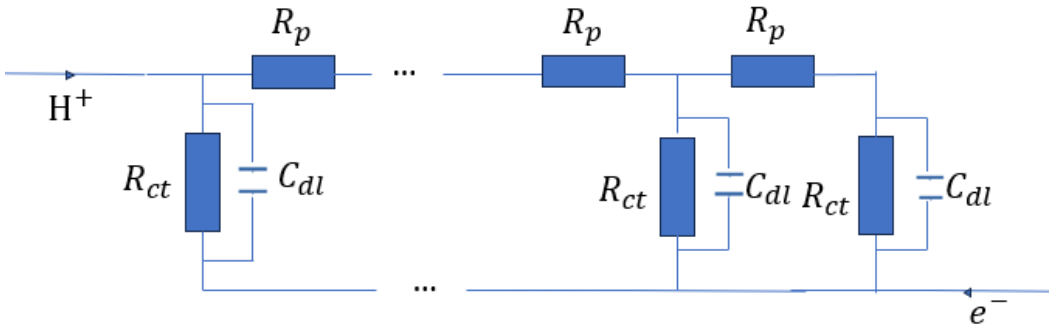


**Figure 12** Transmission Line representation of the CCL including protonic-resistivity ($R_p$), double-layer capacitor ($C_{dl}$), along with the charge transfer resistance ($R_{ct}$).

From this transmission line, the numerical impedance of the CCL can be computed iteratively, from the right (GDL/CCL interface) to the left (CCL/Membrane interface). We have at the $N$th element an open-circuit, then the impedance is,

$$Z_{ccl,\,N} = Z_{ct,\,N} + R_p. \qquad 3\text{-}1$$

For $k = N, \ldots, 2$ ,

$$Z_{ccl,\,k-1} = \left(\frac{1}{Z_{ccl,\,k}} + \frac{1}{Z_{ct,k}}\right)^{-1} + R_p, \qquad 3\text{-}2$$

where,

$$Z_{ct,k} = \left(\frac{1}{R_{ct,k}} + j\omega C_{dl}\delta x\right)^{-1}. \qquad 3\text{-}3$$

$Z_{ct,k}$ is the impedance equivalent of the charge transfer resistivity in parallel with the double layer capacitor and $\delta x$ ($\delta x = l_t/N$) is the thickness of each single element,

$$R_p = \frac{\delta x}{\sigma_p}, \qquad 3\text{-}4$$

$$R_{ct} = \frac{b}{\delta j(x)}. \qquad 3\text{-}5$$

The current distribution $j(x)$ across the thickness of the CCL is assumed to be linear (more detailed description of the current distribution is provided in section 3.1.2), $\delta j(x)$ is the current density in a single element. And then the impedance of the CCL (the $N$ elements) is given by,

$$Z_{ccl} = \left(\frac{1}{Z_{ccl,2}} + \frac{1}{Z_{ct,1}}\right)^{-1}. \qquad 3\text{-}6$$

Here the subscripts 1 and 2 indicate the elements of the CCL numbered from 1 (Membrane/CCL interface) till $N$ (CCL/GDL interface). A more detailed description of this segmentation is available in [72].

Figure 13 shows a mutual understanding of the two models (TLM and analytical model). They give same results.

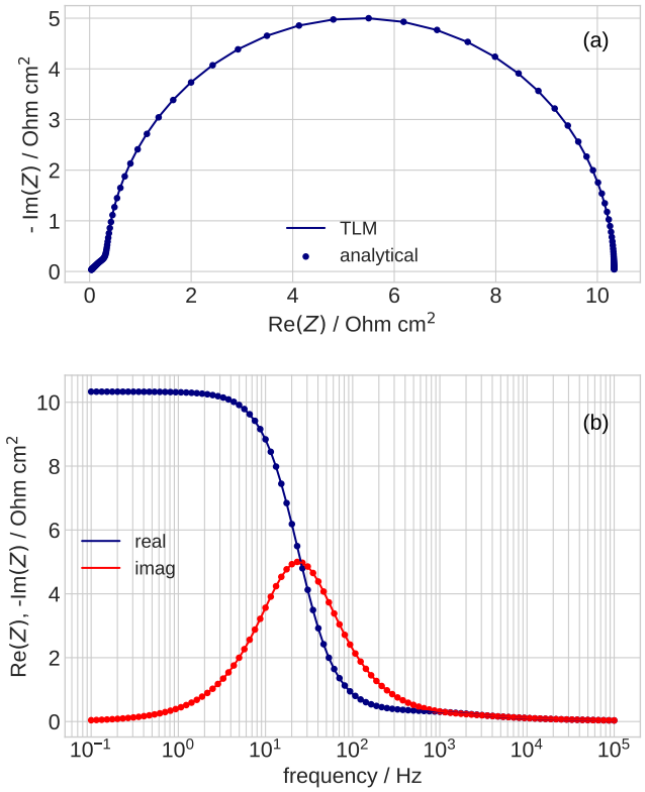


**Figure 13** Impedance spectra of the transmission line model (Solid line -) (Eq. 3-6) compared with the analytical impedance of the CCL (points) Eq. 2-10 for the parameters in Table 4: (a)Nyquist spectrum and (b) Frequency dependence of the real and imaginary parts of the spectrum in (a).

The Nyquist spectrum shows a semi-circle (characterizing the processes of double layer charging) linked with a straight line in the high frequency region. This straight line is more visible in the Bode plot (Figure 13) accounting for proton transport in the CCL.

### 3.1.1.1 SENSITIVITY ANALYSIS

Kulikovsky and Eikerling [15], in their work have simulated the analytical impedance with different values of $\tilde{j}_0^0$ (and confirmed with experimental results from [64]) which showed us the dependance of the analytical impedance on the dimensionless static current density. The larger is the current density, the smaller is the semi-circle in the Nyquist spectra.

Here we perform a sensitivity analysis of the analytical solution of Kulikovsky and Eikerling [15] using the relative sensitivity defined in the previous chapter with respect to the applied current density,

$$S_R = \frac{\delta|\tilde{Z}|/|\tilde{Z}|}{\delta\tilde{j}_0^0/\tilde{j}_0^0}, \qquad 3\text{-}7$$

$$\frac{\delta\tilde{j}_0^0}{\tilde{j}_0^0} = 0.05, \quad 3\text{-}8$$

$$\delta|\tilde{Z}| = |\tilde{Z}_{\delta\tilde{j}_0^0+\tilde{j}_0^0}| - |\tilde{Z}_{\tilde{j}_0^0}|, \quad 3\text{-}9$$

$$|\tilde{Z}| = |\tilde{Z}_{\tilde{j}_0^0}|. \quad 3\text{-}10$$

Figure 14 illustrates that this model has a higher sensitivity at the frequencies below 1Hz in terms of current density and over 100Hz, the relative sensitivity is almost zero (0).

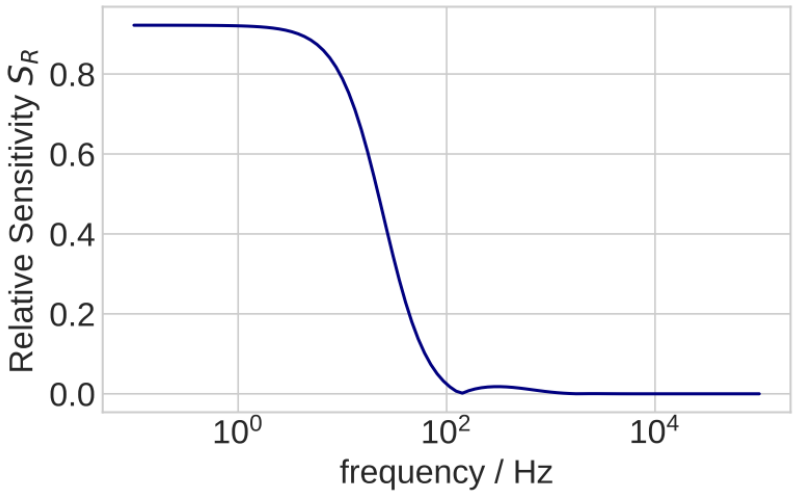


**Figure 14** Sensitivity of the analytical impedance in term of $\tilde{j}_0^0$.

Therefore, to know the best frequency for current density measurement, accurate sensitivity analysis (e.g., calculating the relative sensitivity) is needed.

### 3.1.1.2 CONTROLLABILITY AND OBSERVABILITY

Controllability and observability are based on these state space equations,

$$\frac{dX}{dt} = AX + BW, \quad 3\text{-}11$$

$$Y = CX + DW. \quad 3\text{-}12$$

The variables in this system of equations are well defined in the previous chapter. From this system, a transfer is derived (Eq. 2-20) followed by a residual matrix (Eq. 2-24). For the model used in this research, we have only one input and output,

$$\frac{\partial\tilde{\eta}}{\partial\tilde{t}} + \varepsilon^2\frac{\partial\tilde{j}}{\partial\tilde{x}} = -\tilde{c}\,sinh\,\tilde{\eta}, \quad 3\text{-}13$$

$$\tilde{j} = -\frac{\partial\tilde{\eta}}{\partial\tilde{x}}, \quad 3\text{-}14$$

leading to,

$$\varepsilon^2 \frac{\partial^2 \tilde{\eta}^1}{\partial \tilde{x}^2} = (\tilde{c} \cosh \tilde{\eta}^0 + i\tilde{\omega})\tilde{\eta}^1. \qquad 3\text{-}15$$

Hence, the linear system theory is not applicable to this specific model: the most important processes in the CCL can be modelled with the current, voltage and the oxygen concentration (the case of this model). However, utilizing only these variables (low number of variables) does not yield matrixes in the end.

Furthermore, the model incorporates a spatial derivative in the ODEs, which does not appear in the mathematical framework of linear systems for controllability and observability assessment. Although we could discretize and get matrixes for local values (representing each segment or slice of electrode), but these local values are neither controllable, nor observable; this model is valid in the regime of low current densities where the static overpotential is nearly independent of *x* (its local values are nearly the same). What we can control or observe are mostly the boundary values/conditions: overpotential at position 0 (membrane/CCL interface), total current, concentration at the channel inlet or outlet. However, these boundary conditions are not considered in the formalism of the method.

The linear system theory is not a suitable approach for controllability and observability characterization of these types of models.

### 3.1.2 PEFC MODEL CONSIDERING OXYGEN TRANSPORT

Taking oxygen transport into account, the performance of the CCL can be characterized using the following equations [47]:

Charge conservation:

$$C_{dl} \frac{\partial \eta}{\partial t} + \frac{\partial j}{\partial x} = -i_* \left(\frac{c}{c_{ref}}\right) exp\left(\frac{\eta}{b}\right), \qquad 3\text{-}16$$

Ohm's Law:

$$j = -\sigma_p \frac{\partial \eta}{\partial x}, \qquad 3\text{-}17$$

Mass conservation:

$$\frac{\partial c}{\partial t} - D_{ox} \frac{\partial^2 c}{\partial x^2} = -\frac{i_*}{4F} \left(\frac{c}{c_{ref}}\right) exp\left(\frac{\eta}{b}\right). \qquad 3\text{-}18$$

Combining this set of equations, Kulikovsky [47] reported an analytical impedance response of the CCL including oxygen transport. The resulting impedance is given in the dimensionless form as the following:

$$\tilde{Z}_{ccl} = \frac{A_1}{B_1}, \qquad 3\text{-}19$$

$$A_1 = 4\varphi_1\varphi_2(2ps + (q-r)^2)\cosh\left(\frac{\varphi_1}{2}\right)\cosh\left(\frac{\varphi_2}{2}\right) + 8ps\left(2(q+r)\sinh\left(\frac{\varphi_1}{2}\right)\sinh\left(\frac{\varphi_2}{2}\right) + \varphi_1\varphi_2\right), \quad 3\text{-}20$$

$$B_1 = \varphi_1\cosh\left(\frac{\varphi_1}{2}\right)\sinh\left(\frac{\varphi_2}{2}\right) * \left(\left(2ps + (q-r)(q-r-\psi)\right)\varphi_2^2 + 4ps(q+r-\psi)\right) + \varphi_2\sinh\left(\frac{\varphi_1}{2}\right)\cosh\left(\frac{\varphi_2}{2}\right) * \left(\left(2ps + (q-r)(q-r+\psi)\right)\varphi_1^2 + 4ps(q+r+\psi)\right), \quad 3\text{-}21$$

$$\psi = \sqrt{4ps + (q-r)^2}, \quad 3\text{-}22$$

$$\varphi_1 = \sqrt{2(q+r) + 2\psi}, \quad 3\text{-}23$$

$$\varphi_2 = \sqrt{2(q+r) - 2\psi}, \quad 3\text{-}24$$

$$r = \frac{e^{\tilde{\eta}_0} + i\tilde{\omega}\mu^2}{\varepsilon^2\widetilde{D}_{ox}}, \quad 3\text{-}25$$

$$s = \frac{\tilde{c}_1^0 e^{\tilde{\eta}_0}}{\varepsilon^2\widetilde{D}_{ox}}, \quad 3\text{-}26$$

$$p = \frac{e^{\tilde{\eta}_0}}{\varepsilon^2}, \quad 3\text{-}27$$

$$q = \frac{\tilde{c}_1^0 e^{\tilde{\eta}_0} + i\tilde{\omega}}{\varepsilon^2}, \quad 3\text{-}28$$

$$e^{\tilde{\eta}_0} = \varepsilon^2\frac{\tilde{J}_0}{\tilde{c}_1^0}, \quad 3\text{-}29$$

$$\mu = \sqrt{\frac{4Fc_{ref}}{C_{dl}b}}. \quad 3\text{-}30$$

In this thesis work, a TLM is constructed (Figure 15) to calculate the impedance response of the CCL taking into account oxygen transport and compared with the physical result of Kulikovsky [47].

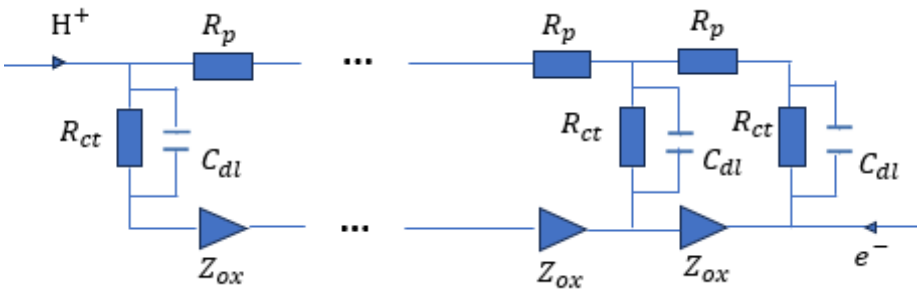


**Figure 15** Transmission line model consisting of protonic-resistivity ($R_p$), double-layer capacitor ($C_{dl}$), along with the charge transfer resistance ($R_{ct}$) and the Warburg impedance ($Z_{ox}$).

Consider the simplified transmission line (see Figure 15), where the CCL is segmented into $n$ ($n = 50$) elements (sub-layers). Each element is formed by a proton resistivity ($R_p$) associated with the proton transport in the sub-layer, a charge transfer resistivity ($R_{ct}$) during oxygen reduction reaction (ORR), connected in parallel with the double layer capacitor ($C_{dl}$) characterizing the effects of double layer charging (electrochemical reaction), and the corrected Warburg element ($Z_{ox}$) standing for the resistance of the CCL sub-layer due to diffusion processes of oxygen molecules. These RC-circuit elements replicate continuously the electrical networking within the CCL. Thus, the impedance response of the CCL can be calculated iteratively (from the GDL/CCL interface to the CCL/membrane interface) as follows:

$$Z_n = Z_{ct,n} + Z_{ox,n} + R_p, \tag{3-31}$$

$$Z_{ox} = \frac{b\tanh\left(\delta x\sqrt{i\omega/D_{ox}}\right)}{(1 + i\omega C_{dl}\delta x b/\delta j(x))4Fc_{ref}\sqrt{i\omega D_{ox}}}, \tag{3-32}$$

$$Z_{ct} = \left(\frac{1}{R_{ct}} + i\omega C_{dl}\delta x\right)^{-1}, \tag{3-33}$$

where $Z_n$ is the impedance of the last single element (at CCL/GDL interface) which stands as an open circuit, $Z_{ox}$, characterizing the finite diffusion processes of oxygen molecules in the CCL, is the Warburg finite-length impedance corrected by Kulikovsky [73], and $\delta x = l_t/n$, $l_t$ is the thickness of the CCL.

For $k = n, \ldots, 2$,

$$Z_{k-1} = \left(\frac{1}{Z_k} + \frac{1}{Z_{ct,k-1}}\right)^{-1} + Z_{ox,k-1} + R_p, \tag{3-34}$$

where $Z_1$ is the impedance of the cell CCL. The protonic and charge transfer resistivities can be computed, respectively as:

$$R_p = \frac{\delta x}{\sigma_p}, \qquad 3\text{-}35$$

$$R_{ct} = \frac{b}{\delta j(x)}. \qquad 3\text{-}36$$

Contained in Table 5 are the parameters utilized in simulating equations 3-34 and 3-19, as indicated in Figure 17.

**Table 5:** Physical Parameters.

| | |
|---|---|
| Tafel slope $b$ , V | 0.03 |
| Proton conductivity $\sigma_p$ , $\Omega^{-1}$ cm$^{-1}$ | 0.01 |
| Exchange current density $i_*$ , A cm$^{-3}$ | $10^{-3}$ |
| CL capacitance $C_{dl}$ , F cm$^{-3}$ | 20 |
| CL thickness $l_t$ , cm | $10^{-4}$ |
| Cell current density $j_0$ , A cm$^{-2}$ | 0.1 |
| CCL oxygen diffusivity $D_{ox}$, cm$^2$ s$^{-1}$ | $2 \times 10^{-4}$ |
| Cell Temperature $T$, K | $273 + 80$ |

The current distribution $j(x)$ is assumed to have a linear shape (as depicted in Figure 16) through the CCL thickness,

$$j(x) = j_0\left(1 - \frac{\delta x}{l_t}\right), \qquad 3\text{-}37$$

and $\delta j(x) = j_{k+1} - j_k$ is the local current density in the $k$th TLM element. The static shape of the overpotential is nearly independent of the distance from the membrane. These assumptions are valid as long as the current density is sufficiently small, typically below 100 mA cm$^{-2}$ [47].

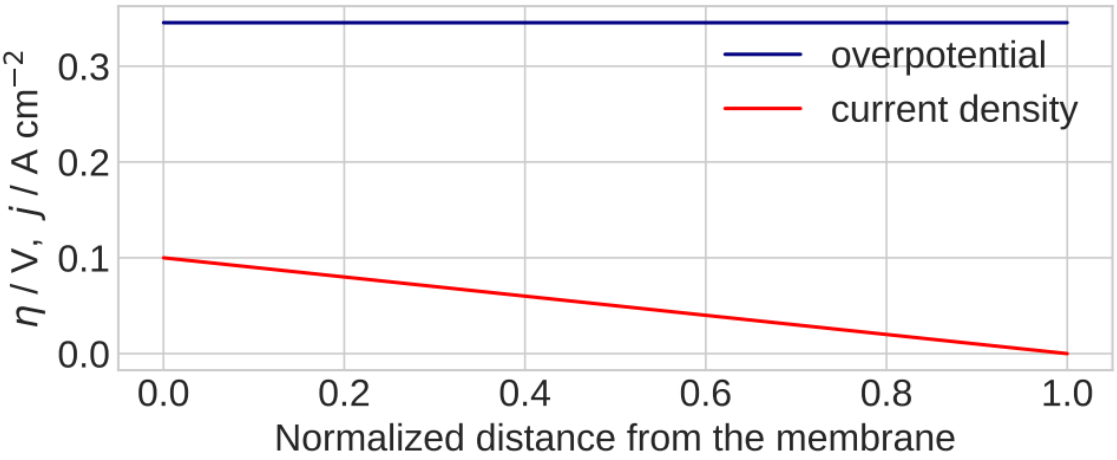


**Figure 16** Static shapes of the local proton current density and the overpotential through the CCL.

Figure 17 shows a perfect agreement between the two methods, the analytical model and the transmission line model yield identical results.

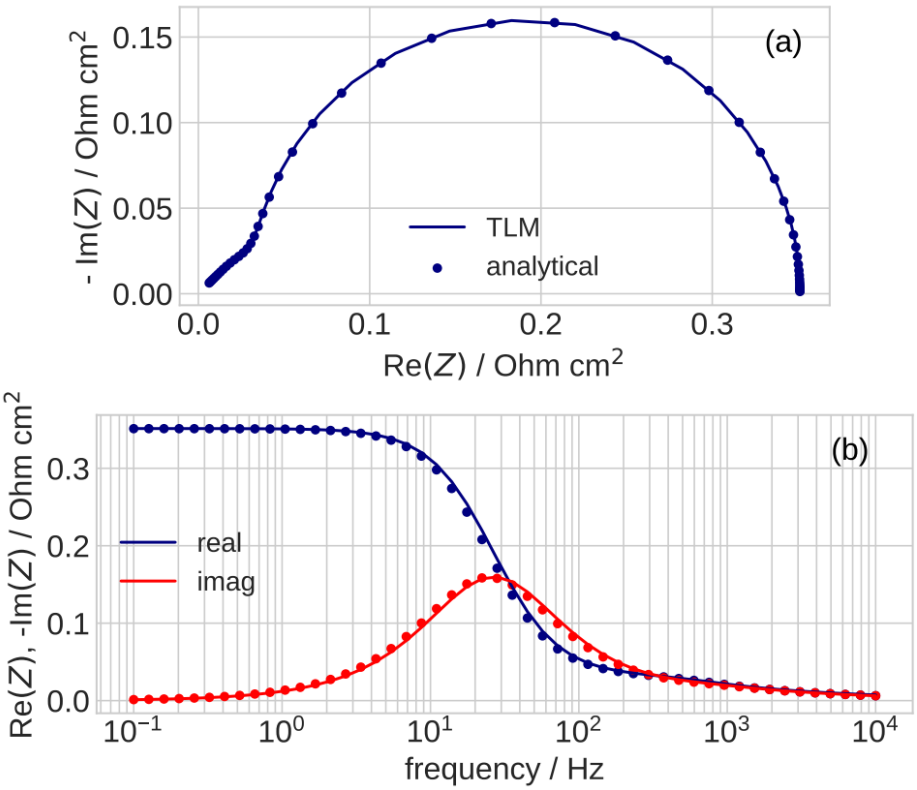


**Figure 17** Impedance spectra of the transmission line model (Solid line −) (Eq. 3-34) for the parameters in Table 5, compared with the analytical impedance of the CCL (points) Eq. 3-19: (a)Nyquist plot and (b) Frequency dependence of the real and imaginary parts of the spectrum in (a).

The Nyquist spectrum is composed of a semi-circle linked with a straight line in the high frequency region (see Figure 17). This straight line highly depends on the proton conductivity. If the latter increases (up to $\sigma_p = 0.05\,\Omega^{-1}\mathrm{cm}^{-1}$) the visibility of this straight line (associated with the proton transport in the CCL) decreases considerably. This can be easily seen in Figure 18.

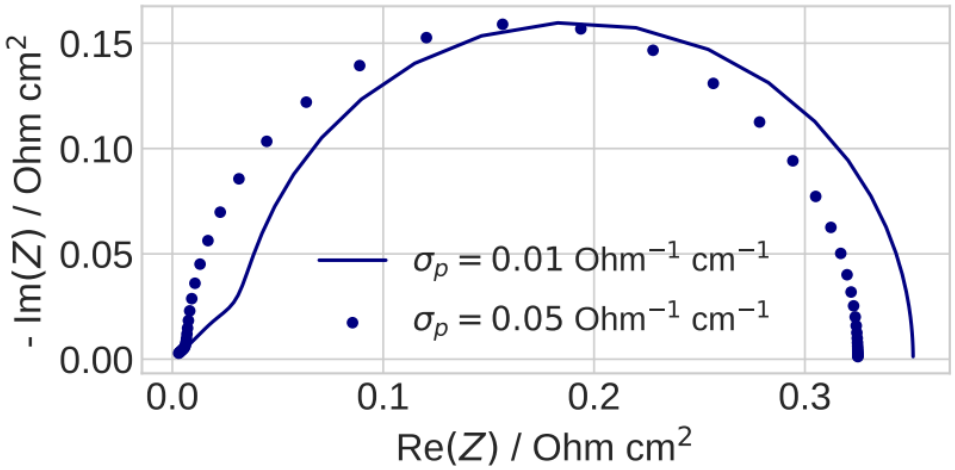


**Figure 18** Nyquist spectrum of Eq. 3-34 simulated with different values of the proton conductivity ($\sigma_p = 0.01\ \Omega^{-1}\text{cm}^{-1}$ (Solid line) and $\sigma_p = 0.05\ \Omega^{-1}\text{cm}^{-1}$ (points)).

On the other hand, Figure 19 shows the effect of oxygen diffusivity on the impedance spectrum. The oxygen diffusivity $D_{ox}$ does not really affect the straight line, but there is a noticeable increase in the diameter of the semi-circle as the oxygen diffusivity coefficient in the CCL decreases. The semi-circle is related to the processes of double layer charging and oxygen diffusion. Note that $D_{ox}$ is maintained within the range of $1 \times 10^{-4}$ to $1 \times 10^{-3}$ cm$^2$ s$^{-1}$.

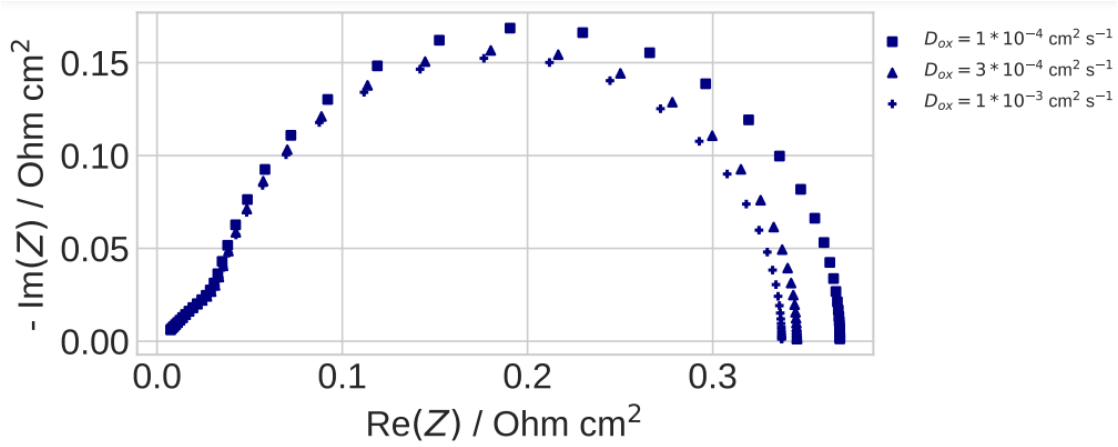


**Figure 19** Eq. 3-34 simulated with different values of the CCL oxygen diffusivity $D_{ox}$.

A sensitivity analysis is performed (Figure 20) by computing the relative sensitivity with respect to the proton conductivity and the oxygen diffusivity (as done in Section 3.1.1.1).

Figure 20 shows that the model has a higher sensitivity to changes in proton conductivity compared to changes in oxygen diffusivity.

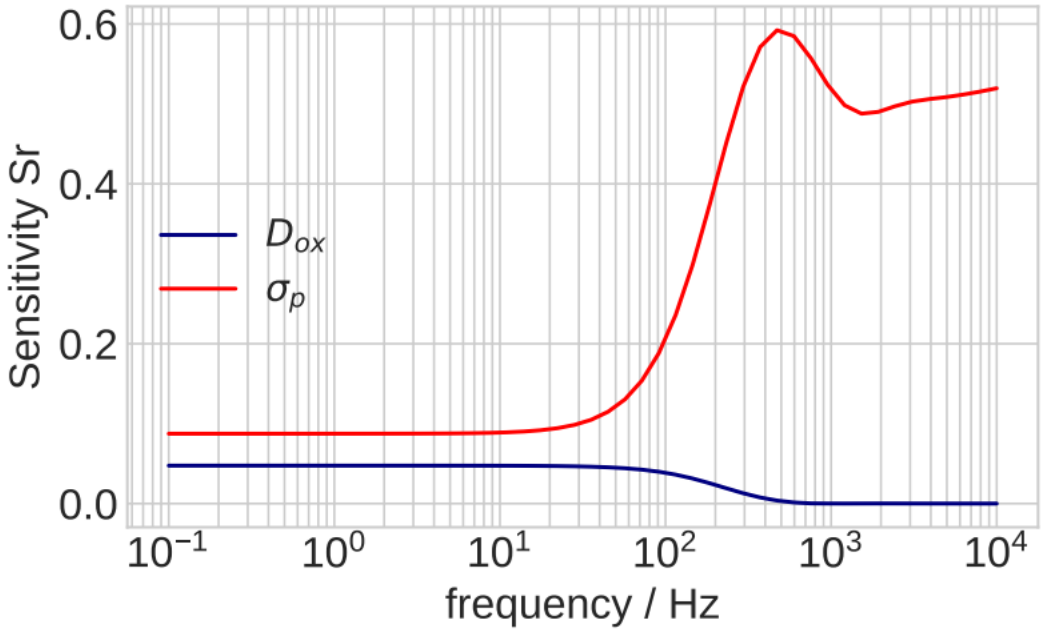


**Figure 20** Sensitivity of the analytical impedance in term of $D_{ox}$ and $\sigma_p$.

At frequencies below 100 Hz, the model shows higher sensitivity towards variations in oxygen diffusivity. Beyond $10^3$ Hz, the relative sensitivity in terms of oxygen diffusivity becomes zero, as oxygen diffusion is a slower process that cannot follow the fast perturbation and is in a dynamic steady state at these frequencies. In contrast, the model displays higher sensitivity in the high frequency region (above 100 Hz) concerning proton conductivity, reaching its peak between 100 Hz and $10^3$ Hz. At the frequencies below 10 Hz, the sensitivity in terms of proton conductivity is low (approximately 0.1 in relative sensitivity).

## PARTIAL CONCLUSION

The use of the suggested linear system theory framework, using controllability and observability matrices, is not a suitable approach for these types of models. This limitation arises from the PEFC models' low number of state variables and their spatial distribution. However, sensitivity analysis using relative sensitivity, shows that the model is almost only sensitive to changes in current density in the low frequency region (below 100 Hz).

To numerically compute the impedance response of the CCL, we used a transmission line model, which yield same result as the analytical approach. Additionally, we extended our work by constructing a transmission line model considering oxygen transport in the CCL for low current density, and find a perfect alignment with an existing physical model. The model is used to evaluate the effects of oxygen diffusivity and proton conductivity in the impedance spectrum: variations in proton conductivity significantly influence the straight line in the high

frequency region while changes in oxygen diffusivity affect only the semi-circle in the impedance spectrum. We further calculate relative sensitivities with respect to oxygen diffusivity and proton conductivity, revealing that the model is more sensitive to changes in proton conductivity than oxygen diffusivity. Oxygen diffusivity sensitivity is limited to the low frequency region (below 1000 Hz), whereas proton conductivity has a maximum sensitivity between 100 and 1000 Hz.

# CONCLUSION AND PERSPECTIVES

# CONCLUSION AND PERSPECTIVES

The PEFC is the most widely studied technology among fuel cells due to its simplicity, viability, quick start-up, high energy conversion efficiency, low operating temperature, high current density, zero emissions and flexible useability in various applications. Nevertheless, the use of accurate diagnostic techniques is crucial to ensure their reliable operation and optimal performance. For this purpose, to find the best FRA method or combined methods for PEFC analysis, the model-based analysis of controllability, observability, and the parameter sensitivity is a suitable approach, it helps in evaluating the strengths and weaknesses of a given or combination of methods.

A detailed literature review was conducted in this thesis, providing an overview of the different type of fuel cells on which researchers are more focused. PEFC was subsequently introduced in detail, providing a comprehensive overview of its structure, working principle, and dynamics as well as frequency response diagnostic techniques such as electrochemical impedance spectroscopy, electrochemical pressure impedance spectroscopy, concentration-alternating frequency response analysis, and concentration admittance spectroscopy.

Firstly, we utilized an existing analytical solution of a simple EIS model of the CCL to characterize observability, controllability, and parameter sensitivity (relative sensitivity introduced in recent works is used) of the system. It is noticeable that the suggested linear system theory framework, using controllability and observability matrices, is not suitable for these types of models because PEFC models have only a small number of relevant state variables, are spatially distributed and the input and output signals are often contained in the boundaries rather than the state variables, which hinders the suggested mathematical treatment. However, relative sensitivities are measures that are easy to compute, straightforward to understand and interpret and give useful and practical insights into the parameters of the model.

In addition to the simple analytical model, a transmission line model of the CCL is used to numerically efficiently calculate the impedance response, which matches the analytical solution. Furthermore, we extended our analysis by constructing a transmission line model that accounts for oxygen transport in the CCL for low current density, which has a good agreement with an available physical model. The model is used to analyze effects of the oxygen diffusivity and proton conductivity in the spectrum. The straight line in the high frequency region is affected by proton conductivity. If the latter increases, the straight line becomes more difficult to notice. The oxygen diffusivity has effect only on the semi-circle, which increase in diameter with the decrease in oxygen diffusivity. A sensitivity analysis of the model in terms of oxygen

diffusivity and proton conductivity reveals that oxygen diffusivity is only sensitive in the low frequency region, while proton conductivity has a maximum sensitivity in the intermediate frequency range.

In this thesis, a model-based analysis of controllability, observability and parameter sensitivity was presented as a tool for identifying the best FRA method or combined methods using an analytical solution. However, the approach used in our work is not directly applicable to these types of models and further development or research into different methods are necessary. Additionally, this model can be expanded in a water-saturation-dependent description of the proton conductivity, which might allow extracting water saturation properties from measured impedance spectra.

# BIBLIOGRAPHY REFERENCES

[1] S. Barca, “Energy, property, and the industrial revolution narrative,” *Ecological Economics*, vol. 70, no. 7, pp. 1309–1315, 2011.

[2] S. Lange, J. Pohl, and T. Santarius, “Digitalization and energy consumption. Does ICT reduce energy demand?,” *Ecological economics*, vol. 176, p. 106760, 2020.

[3] F. Chien, L. Huang, and W. Zhao, “The influence of sustainable energy demands on energy efficiency: Evidence from China,” *Journal of Innovation & Knowledge*, vol. 8, no. 1, p. 100298, 2023.

[4] D. Bodansky, “Paris Agreement, United Nations Audiovisual Library of International Law,” 2021.

[5] INTERGOVERNMENTAL PANEL ON CLIMATE CHANGE, *Climate Change 2014: Synthesis Report (Longer Report)*. Intergovernmental Panel on Climate Change, 2014.

[6] P. García, C. A. García, L. M. Fernández, F. Llorens, and F. Jurado, “ANFIS-based control of a grid-connected hybrid system integrating renewable energies, hydrogen and batteries,” *IEEE Transactions on industrial informatics*, vol. 10, no. 2, pp. 1107–1117, 2013.

[7] G. Wang, L. Zhang, and J. Zhang, “A review of electrode materials for electrochemical supercapacitors,” *Chemical Society Reviews*, vol. 41, no. 2, pp. 797–828, 2012.

[8] P. Bujlo, G. Pasciak, J. Chmielowiec, and M. Malinowski, “Application of a polymer exchange membrane fuel cell stack as the primary energy source in a commercial uninterruptible power supply unit,” *Journal of Power Technologies*, vol. 93, no. 3, pp. 154–160, 2013.

[9] T. Kadyk, Y. Sun, J. Kaur, A. Kulikovsky, and M. Eikerling, “Frequency response diagnostics of electrochemical energy devices,” *Current Opinion in Electrochemistry*, 2023.

[10] A. Sorrentino, K. Sundmacher, and T. Vidakovic-Koch, “Polymer electrolyte fuel cell degradation mechanisms and their diagnosis by frequency response analysis methods: A review,” *Energies*, vol. 13, no. 21, p. 5825, 2020.

[11] D. Grübl, J. Janek, and W. G. Bessler, “Electrochemical Pressure Impedance Spectroscopy (EPIS) as diagnostic method for electrochemical cells with gaseous reactants: A model-based analysis,” *Journal of the Electrochemical Society*, vol. 163, no. 5, p. A599, 2016.

[12] F. Kubannek and U. Krewer, “Studying the interaction of mass transport and electrochemical reaction kinetics by species frequency response analysis,” *Journal of The Electrochemical Society*, vol. 167, no. 14, p. 144510, 2020.

[13] Y. Sun, T. Kadyk, A. Kulikovsky, and M. Eikerling, “A model for the concentration admittance of a polymer electrolyte fuel cell,” *The Journal of Physical Chemistry C*, vol. 126, no. 33, pp. 14075–14081, 2022.

[14] F. Ciucci, T. Carraro, W. C. Chueh, and W. Lai, “Reducing error and measurement time in impedance spectroscopy using model based optimal experimental design,” *Electrochimica Acta*, vol. 56, no. 15, pp. 5416–5434, 2011.

[15] A. Kulikovsky and M. Eikerling, “Analytical solutions for impedance of the cathode catalyst layer in PEM fuel cell: Layer parameters from impedance spectrum without fitting,” *Journal of Electroanalytical Chemistry*, vol. 691, pp. 13–17, 2013.

[16] W. R. Grove, “XXIV. on voltaic series and the combination of gases by platinum,” *The London, Edinburgh, and Dublin Philosophical Magazine and Journal of Science*, vol. 14, no. 86-87, pp. 127–130, 1839.

[17] D. Hissel and M.-C. Pera, “Diagnostic & health management of fuel cell systems: Issues and solutions,” *Annual Reviews in Control*, vol. 42, pp. 201–211, 2016.

[18] J. Larminie and A. Dicks, “Fuel cell systems explained,” *J. Wiley*, vol. 2, pp. 67–117, 2003.

[19] Y. Wang, K. S. Chen, J. Mishler, S. C. Cho, and X. C. Adroher, “A review of polymer electrolyte membrane fuel cells: Technology, applications, and needs on fundamental research,” *Applied energy*, vol. 88, no. 4, pp. 981–1007, 2011.

[20] L. Wang, A. Husar, T. Zhou, and H. Liu, “A parametric study of PEM fuel cell performances,” *International journal of hydrogen energy*, vol. 28, no. 11, pp. 1263–1272, 2003.

[21] H. Pourrahmani, M. Siavashi, A. Yavarinasab, M. Matian, N. Chitgar, L. Wang, and J. Van Herle, “A review on the long-term performance of proton exchange membrane fuel cells: From degradation modeling to the effects of bipolar plates, sealings, and contaminants,” *Energies*, vol. 15, no. 14, p. 5081, 2022.

[22] Office of Fossil Energy United States Department of Energy. “Fuel Cell Handbook (Seventh Edition),” *National Energy Technology Laboratory*, 2004.

[23] X. Li and I. Sabir, “Review of bipolar plates in pem fuel cells: Flow-field designs,” *International journal of hydrogen energy*, vol. 30, no. 4, pp. 359–371, 2005.

[24] E. O. Balogun, “Comparative analysis of polymer electrolyte membrane (PEM) fuel cells,” master’s thesis, University Of Cape Town, 2018.

[25] N. Bevilacqua, T. Asset, M. Schmid, H. Mark ̈otter, I. Manke, P. Atanassov, and R. Zeis, “Impact of catalyst layer morphology on the operation of high temperature PEM fuel cells,” *Journal of Power Sources Advances*, vol. 7, p. 100042, 2021.

[26] Z. Luo, Z. Chang, Y. Zhang, Z. Liu, and J. Li, “Electro-osmotic drag coefficient and proton conductivity in Nafion® membrane for PEMFC,” *International Journal of Hydrogen Energy*, vol. 35, no. 7, pp. 3120–3124, 2010.

[27] A. Abaspour, N. T. Parsa, and M. Sadeghi, “A new feedback Linearization-NSGA-II based control design for PEM fuel cell,” *International Journal of Computer Applications*, vol. 97, no. 10, 2014.

[28] T. Muzaffar, T. Kadyk, and M. Eikerling, “Tipping water balance and the Pt loading effect in polymer electrolyte fuel cells: a model-based analysis,” *Sustainable Energy & Fuels*, vol. 2, no. 6, pp. 1189–1196, 2018.

[29] M. Eikerling, A. A. Kornyshev, and A. R. Kucernak, “Water in polymer electrolyte fuel cells: Friend or foe?,” *Physics Today*, vol. 59, no. 10, pp. 38–44, 2006.

[30] D. L. Wood III, J. Chlistunoff, J. Majewski, and R. L. Borup, “Nafion structural phenomena at platinum and carbon interfaces,” *Journal of the American Chemical Society*, vol. 131, no. 50, pp. 18096–18104, 2009.

[31] J. Aubry, N. Y. Steiner, S. Morando, N. Zerhouni, and D. Hissel, “Fuel cell diagnosis methods for embedded automotive applications,” *Energy Reports*, vol. 8, pp. 6687–6706, 2022.

[32] M. Ordonez, M. O. Sonnaillon, J. E. Quaicoe, and M. T. Iqbal, “An embedded frequency response analyzer for fuel cell monitoring and characterization,” *IEEE Transactions on Industrial Electronics*, vol. 57, no. 6, pp. 1925–1934, 2009.

[33] O. Antoine, Y. Bultel, and R. Durand, “Oxygen reduction reaction kinetics and mechanism on platinum nanoparticles inside nafion®,” *Journal of Electroanalytical Chemistry*, vol. 499, no. 1, pp. 85–94, 2001.

[34] M. Eikerling and A. Kornyshev, “Electrochemical impedance of the cathode catalyst layer in polymer electrolyte fuel cells,” *Journal of Electroanalytical Chemistry*, vol. 475, no. 2, pp. 107–123, 1999.

[35] T. Springer, T. Zawodzinski, M. Wilson, and S. Gottesfeld, “Characterization of polymer electrolyte fuel cells using ac impedance spectroscopy,” *Journal of the Electrochemical Society*, vol. 143, no. 2, p. 587, 1996.

[36] J. Wu, X. Z. Yuan, H. Wang, M. Blanco, J. J. Martin, and J. Zhang, “Diagnostic tools in PEM fuel cell research: Part I electrochemical techniques,” *International Journal of Hydrogen Energy*, vol. 33, no. 6, pp. 1735–1746, 2008.

[37] A. C. Lazanas and M. I. Prodromidis, “Electrochemical impedance spectroscopy a tutorial,” *ACS Measurement Science Au*, 2023.

[38] J. Collet-Lacoste, “The electrochemical impedance spectroscopy and associated transfer functions: Non-equilibrium thermodynamics consideration,” *Electrochimica Acta*, vol. 49, no. 27, pp. 4967–4977, 2004.

[39] S. M. R. Niya and M. Hoorfar, “Study of proton exchange membrane fuel cells using electrochemical impedance spectroscopy technique–a review,” *Journal of Power Sources*, vol. 240, pp. 281–293, 2013.

[40] W. Choi, H.-C. Shin, J. M. Kim, J.-Y. Choi, and W.-S. Yoon, “Modeling and applications of electrochemical impedance spectroscopy (EIS) for lithium-ion batteries,” *Journal of Electrochemical Science and Technology*, vol. 11, no. 1, pp. 1–13, 2020.

[41] A. Sorrentino, T. Vidakovic-Koch, R. Hanke-Rauschenbach, and K. Sundmacher, “Concentration-alternating frequency response: A new method for studying polymer electrolyte membrane fuel cell dynamics,” *Electrochimica Acta*, vol. 243, pp. 53–64, 2017.

[42] A. M. Niroumand, W. Mérida, M. Eikerling, and M. Saif, “Pressure–voltage oscillations as a diagnostic tool for PEFC cathodes,” *Electrochemistry communications*, vol. 12, no. 1, pp. 122–124, 2010.

[43] P. Hartmann, D. Grubl, H. Sommer, J. Janek, W. G. Bessler, and P. Adelhelm, “Pressure dynamics in metal-oxygen (metal-air) batteries: a case study on sodium superoxide cells,” *The Journal of Physical Chemistry C*, vol. 118, no. 3, pp. 1461–1471, 2014.

[44] A. Kulikovsky, “Electrochemical pressure impedance spectroscopy for PEM fuel cells: Are the measured spectra unique?,” *Journal of The Electrochemical Society*, vol. 169, no. 9, p. 094513, 2022.

[45] E. Engebretsen, T. J. Mason, P. R. Shearing, G. Hinds, and D. J. Brett, “Electrochemical pressure impedance spectroscopy applied to the study of polymer electrolyte fuel cells,” *Electrochemistry Communications*, vol. 75, pp. 60–63, 2017.

[46] A. Baricci and A. Casalegno, “Experimental analysis of catalyst layer operation in a high-temperature proton exchange membrane fuel cell by electrochemical impedance spectroscopy,” *Energies*, vol. 16, no. 12, p. 4671, 2023.

[47] A. Kulikovsky, “Analytical impedance of PEM fuel cell cathode including oxygen transport in the channel, gas diffusion, and catalyst layers,” *Journal of The Electrochemical Society*, vol. 169, no. 3, p. 034527, 2022.

[48] A. Kulikovsky, “One-dimensional impedance of the cathode side of a PEM fuel cell: Exact analytical solution,” *Journal of The Electrochemical Society*, vol. 162, no. 9, pp. F217-F222, 2015.

[49] T. Reshetenko and A. Kulikovsky, “PEM fuel cell characterization by means of the physical model for impedance spectra,” *Journal of The Electrochemical Society*, vol. 162, no. 7, p. F627, 2015.

[50] M. Cimenti, D. Bessarabov, M. Tam, and J. Stumper, “Investigation of proton transport in the catalyst layer of PEM fuel cells by electrochemical impedance spectroscopy,” *ECS transactions*, vol. 28, no. 23, p. 147, 2010.

[51] Q. Guo and R. E. White, “A steady-state impedance model for a PEMFC cathode,” *Journal of The Electrochemical Society*, vol. 151, no. 4, p. E133, 2004.

[52] F. Jaouen and G. Lindbergh, “Transient techniques for investigating mass-transport limitations in gas diffusion electrodes: I. modeling the cathode,” *Journal of The Electrochemical Society*, vol. 150, no. 12, p. A1699, 2003.

[53] A. Kulikovsky, “The regimes of catalyst layer operation in a fuel cell,” *Electrochimica acta*, vol. 55, no. 22, pp. 6391–6401, 2010.

[54] M. Eikerling and A. Kornyshev, “Modelling the performance of the cathode catalyst layer of polymer electrolyte fuel cells,” *Journal of Electroanalytical Chemistry*, vol. 453, no. 1-2, pp. 89–106, 1998.

[55] S. Cruz-Manzo and R. Chen, “A generic electrical circuit for performance analysis of the fuel cell cathode catalyst layer through electrochemical impedance spectroscopy,” *Journal of Electroanalytical Chemistry*, vol. 694, pp. 45–55, 2013.

[56] J. E. B. Randles, “Kinetics of rapid electrode reactions,” *Discussions of The Faraday Society*, vol. 1, pp. 11–19, 1947.

[57] N. Wagner, “Electrochemical impedance spectroscopy,” in *PEM Fuel Cell Diagnostic Tools*, *CRC Press*, pp. 37–70, 2011.

[58] N. Wagner and E. G ̈ulzow, “Change of electrochemical impedance spectra (EIS) with time during CO-poisoning of the Pt-anode in a membrane fuel cell,” *Journal of Power Sources*, vol. 127, no. 1-2, pp. 341–347, 2004.

[59] G. Li and P. G. Pickup, “Ionic conductivity of PEMFC electrodes: Effect of Nafion loading,” *Journal of the Electrochemical Society*, vol. 150, no. 11, p. C745, 2003.

[60] D. Malevich, E. Halliop, B. A. Peppley, J. G. Pharoah, and K. Karan, “Investigation of charge-transfer and mass-transport resistances in PEMFCs with microporous layer using electrochemical impedance spectroscopy,” *Journal of The Electrochemical Society*, vol. 156, no. 2, p. B216, 2008.

[61] T. Suzuki, H. Murata, T. Hatanaka, and Y. Morimoto, “Analysis of the catalyst layer of polymer electrolyte fuel cells,” *R&D Rev. Toyota CRDL*, vol. 39, no. 3, pp. 33–38, 2003.

[62] M. Eikerling and A. Kornyshev, “Electrochemical impedance of the cathode catalyst layer in polymer electrolyte fuel cells,” *Journal of Electroanalytical Chemistry*, vol. 475, no. 2, pp. 107–123, 1999.

[63] N. Fouquet, C. Doulet, C. Nouillant, G. Dauphin-Tanguy, and B. Ould-Bouamama, “Model based PEM fuel cell state-of-health monitoring via ac impedance measurements,” *Journal of Power Sources*, vol. 159, no. 2, pp. 905–913, 2006.

[64] R. Makharia, M. F. Mathias, and D. R. Baker, “Measurement of catalyst layer electrolyte resistance in PEFCs using electrochemical impedance spectroscopy,” *Journal of The Electrochemical Society*, vol. 152, no. 5, p. A970, 2005.

[65] M. Ciureanu and R. Roberge, “Electrochemical impedance study of PEM fuel cells. experimental diagnostics and modeling of air cathodes,” *The Journal of Physical Chemistry B*, vol. 105, no. 17, pp. 3531–3539, 2001.

[66] S. Touhami, J. Mainka, J. Dillet, S. A. H. Taleb, and O. Lottin, “Transmission line impedance models considering oxygen transport limitations in polymer electrolyte membrane fuel cells,” *Journal of The Electrochemical Society*, vol. 166, no. 15, p. F1209, 2019.

[67] A. Goshtasbi, J. Chen, J. R. Waldecker, S. Hirano, and T. Ersal, “Effective parameterization of PEM fuel cell models—part I: sensitivity analysis and parameter identifiability,” *Journal of the Electrochemical Society*, vol. 167, no. 4, p. 044504, 2020.

[68] X. D. Wang, J. L. Xu, and D. J. Lee, “Parameter sensitivity examination for a complete three-dimensional, two-phase, non-isothermal model of polymer electrolyte membrane fuel cell,” International journal of hydrogen energy, vol. 37, no. 20, pp. 15766–15777, 2012.

[69] W. Tao, C. Min, X. Liu, Y. He, B. Yin, and W. Jiang, “Parameter sensitivity examination and discussion of PEM fuel cell simulation model validation: Part I. Current status of modeling research and model development,” *Journal of Power Sources*, vol. 160, no. 1, pp. 359–373, 2006.

[70] R. E. Kalman, “Contributions to the theory of optimal control,” *Bol. Soc. Mat. Mexicana*, vol. 5, no. 2, pp. 102–119, 1960.

[71] C. Zhao, X. Wang, Z. Liu, and S. Liu, “The observability and controllability metrics of power system oscillations and the applications,” *Frontiers in Energy Research*, vol. 10, p. 1020894, 2023.

[72] T. Gaumont, G. Maranzana, O. Lottin, J. Dillet, L. Gu´etaz, and J. Pauchet, “In operando and local estimation of the effective humidity of PEMFC electrodes and membranes,” *Journal of The Electrochemical Society*, vol. 164, no. 14, p. F1535, 2017.

[73] A. Kulikovsky, “Why impedance of the gas diffusion layer in a PEM fuel cell differs from the Warburg finite-length impedance?,” *Electrochemistry communications*, vol. 84, pp. 28–31, 2017.